International Journal of Mechanical Sciences 231 (2022) 107568

Contents lists available at ScienceDirect

International Journal of Mechanical Sciences

journal homepage: www.elsevier.com/locate/ijmecsci

Analytical solutions of inerter-added sliding isolation structures to ground motions

Songtao Xue [a,c], Li Zhang [a], Liyu Xie [a], Ruifu Zhang [a,b,*], Jianfei Kang [a]

[a] Department of Disaster Mitigation for Structures, Tongji University, Shanghai 200092, China
[b] State Key Laboratory of Disaster Reduction in Civil Engineering, Tongji University, Shanghai 200092, China
[c] Department of Architecture, Tohoku Institute of Technology, Sendai 982-8577, Japan

ARTICLE INFO

Keywords:
Sliding isolation structure
Inerter
Analytical solution
Motion mode

ABSTRACT

Previous studies have proven that adding an inerter to a sliding isolation structure can reduce the isolation displacement without compromising the control effect of the superstructure. However, due to the strong nonlinearity of the sliding isolator, approximate methods or numerical analyses are adopted to investigate inerter-added sliding isolation structures, which hinders the understanding of the inherent working mechanisms of such structures. This study derives exact analytical solutions during both sliding and stick motion states of inerter-added sliding isolation structures under harmonic ground motions and investigates the influence of an additional inerter on the motion states and responses of such structures. The main novelties of this paper are the employment of the inerter technique in a sliding system for performance improvement and explicit expressions of the dynamic responses and motion modes for inerter-added sliding isolation structures that assist in understanding the role of the additional inerter. Differential equations are established for both the stick and sliding motions of inerter-added sliding isolation structures subjected to harmonic ground excitations. The dynamic characteristics of the structure are analyzed, and accurate analytical solutions are derived for structural responses. The explicit forms for the occurrence conditions of three fundamental modes (i.e., the stick-stick, stick-slip and slip-slip modes) for the motion of the inerter-added sliding isolation structures are presented. Based on the derived analytical solutions, extensive parametric analyses are conducted to investigate the influences of the added inerter on the motion modes and responses of sliding isolation structures. By adding an inerter, a decreased natural frequency, a decreased damping ratio and a reduction in ground motion excitation are observed for the vibration of the superstructure in the inerter-added sliding isolation structure compared to that in the sliding isolation structure without an inerter. Furthermore, the inerter causes the slip-slip mode to occur more easily, which is preferred for sliding isolation structures when sliding occurs. An increasing inertance of the inerter is beneficial for reducing isolation displacement in general but contrary to reducing maximum acceleration in some frequency ranges and excitations with large amplitudes. The trade-off between the reduction of isolation displacement and acceleration is recommended for determining the inertance of the inerter in sliding isolation structures.

1. Introduction

Base isolation technologies have been proven to be efficient for protecting primary structures against damaging seismic excitations in the past few decades [1–3]. Using base isolation systems with low lateral stiffness, the dynamic actions transmitted to the superstructures can be significantly reduced and the dynamic responses of the superstructures are mitigated. Since the birth of the base isolation concept, various base isolation devices have been developed. In general, these devices can be classified into two types: elastomeric bearing and sliding isolation systems [2,4]. Among these two isolation techniques, the sliding isolation system outperforms the elastomeric bearing system in terms of effectiveness in a large excitation frequency range [5]. Meanwhile, when the sliding isolation structure is subjected to ground motions, the forces transmitted to the superstructure in a sliding isolation structure are limited to no more than the friction force along the sliding surface [6,7]. Typical sliding isolation systems include the pure-friction system, the friction pendulum system (FPS) [8] and the resilient-friction base

* Corresponding author at: Department of Disaster Mitigation for Structures, Tongji University, Shanghai 200092, China.
E-mail address: zhangruifu@tongji.edu.cn (R. Zhang).

https://doi.org/10.1016/j.ijmecsci.2022.107568
Received 12 April 2022; Received in revised form 21 July 2022; Accepted 21 July 2022
Available online 26 July 2022

isolator (R-FBI) [9]. Among these systems, the pure-friction system is historically the most-original sliding isolation device without any restoring force [10], which was adopted in bridges [11] and some low-rise buildings for earthquake protection [10,12]. The FPS and R-FBI are sliding isolation systems, including restoring force, which have become more popular for application in recent years [4]. In addition, as a siding isolation system, geotechnical seismic isolation techniques using locally available materials such as limestone sand [13], sand-bitumen mixtures [14] and rubber-soil mixtures [15] were developed for structural seismic response mitigation. These techniques are characterized by low cost and simple construction and are of particular significance in developing countries [16–18].

Although the base isolation technique has an excellent effect for structural response suppression, a large displacement is generally induced at the isolation layer under ground excitation due to the low lateral stiffness. This can be an issue that cannot be neglected for the application of base isolation systems in practice considering the auxiliary facilities (e.g., pipeline systems) existing in the isolation layer and adjacent buildings [19]. To reduce the displacement of the isolation layer, additional energy dissipation devices have been proposed in base isolation systems [20]. However, this strategy can cause an increased response of the superstructure. A hybrid control strategy incorporating the tuned mass damper into the base isolation system was also proposed to address the large isolation displacement [21,22]. More input energy is induced due to the additional mass for the base isolation structure under ground motion. Recently, inerter-based technologies have been introduced into the base isolation system to reduce the isolation displacement without increasing the superstructure responses and inducing external energy input owing to the inherent characteristics of the inerter [23–25].

The inerter is a two-terminal device whose reaction force is proportional to the relative acceleration of its two nodes [26–28]. The constant of this proportionality is defined as inertance (also called apparent mass) [26], which represents the apparent mass effect of an inerter. Using an appropriated physical realization (e.g., the ball screw mechanism), the inertance of an inerter can be generated up to an order of thousands of times to its gravitational mass [29]. In addition, the inerter also exhibits a frequency-dependent negative stiffness effect [30,31]. With the characteristics above, the inerter technique is of increasing interest [32–36] to scholars in the field of structural vibration control, and many high-performance inerter-based devices have been developed [37–43]. Employing the apparent mass effect of the inerter, Zhang et al. [44] presented a tuned mass inerter system to achieve the lightweight control of a wind turbine tower. This device is also employed in multi-mode control of the seismic response of the high-rise industrial chimney [45]. Wang et al. [46] proposed a parallel connected inerter to enhance the performance of an active-passive-combined vehicle suspension system. To improve seat comfort, Ning et al. [47] proposed an electromagnetic inerter device with variable inertance and checked the corresponding capacity through both numerical simulations and experimental tests. In terms of reducing the force transmission from the machine to the ground, Zhang et al. [48] presented an additional inerter system and proposed an optimal design strategy based on the closed-form power equation to achieve efficient control. Inerter-based devices have also been utilized for vibration control of practical structures in China and Japan [26,49]. In summary, inerter-based devices have exhibited an extensive vibration control capacity for structures in different fields. Owing to the special characteristics of inerters, this technology has also been proposed for performance enhancement of base-isolated structures regarding the isolation displacement and responses of the superstructure [23,50,51].

By assuming the base-isolated object as a rigid mass, Saitoh [52] proposed a base isolation system combined with an additional inerter to mitigate the isolation displacement. It is found that the addition of an inerter can reduce the natural frequency and the amplitude of seismic excitation for the base isolation system. Consequently, the isolation displacement is determined to be decreasing based on both the analytical and numerical solutions. Simplifying the superstructure with a single degree of freedom (SDOF) system, Ye et al. [53] derived closed-form solutions for the modal characteristics and seismic responses of the base-isolated structure with an additional inerter. They found that there is a critical inertance such that the modal participation factor equals zero. Thus, the modal response induced by the second mode vanishes at the critical inertance. They proposed an optimal range of inertance to accomplish the trade-off for the displacement mitigation of the isolation layer and superstructure. By connecting the inerter with spring, damping and mass elements, inerter systems composed of different mechanical layouts (e.g., the tuned viscous mass damper (TVMD) [54] and the tuned inerter damper (TID) [55]) are proposed for performance improvement of base-isolated structures based on the closed-form design procedures. Note that all the previous studies are concentrated on the base-isolation structures using elastomeric bearing systems with linear behavior (i.e., represented by the spring and dashpot connected in parallel). However, for the sliding isolation system, its mechanical behavior is highly nonlinear due to the hysteretic behavior of the friction force and the existence of different motion states of stick and slippage along the sliding interface [5,56]. Zhao et al. [57] and De Domenico et al. [58] proposed the optimal design of different inerter systems incorporated into FPS isolation structures, and the corresponding seismic performances were also investigated based on the numerical analysis results. In their studies, the stochastic linearization approach was employed to approximately deal with the nonlinear behavior of the FPS represented with the ideal Coulomb friction model, which is only valid when slippage occurs for the sliding isolation system [59]. However, the stick state also exists for a sliding isolator under ground excitation. In addition, unlike the inerter-added base isolation systems with linear behavior whose theoretical investigation has been conducted in depth, there is no analytical solution reported for the sliding isolation system enhanced with an inerter, which can be useful in understanding the working mechanism and making design decisions of this system. For a sliding isolation structure, the analytical solutions that assist in understanding its inherent mechanism have been explored previously. Tsiavos et al. [60] investigated the analytical responses of base-isolated structures with deformable sliding layers under harmonic and pulse ground motions. The influence of the deformability of the sliding layer on the stick-slip behavior ranges, sliding displacement and acceleration responses are included in their studies. Hu and Nakashima [61] derived analytical solutions for the maximum acceleration response of a two-degrees-of-freedom sliding base system under harmonic ground motions. In these studies, the inerter technique was not examined.

The topic of this study is the analytical solution of the inerter-added sliding isolation structures with the goal of performance improvement, which can be beneficial to explore the role the additional inerter played in an inerter-added sliding isolation system. The fundamental system for the sliding isolation technique, i.e., the pure-friction system, with an additional inerter is employed for investigation under harmonic ground motions. Although this system has the limitation of the absence of the restoring force, it contains the critical components of the inerter-added sliding isolation structures, and a corresponding analytical study can provide more in-depth insight into the inherent mechanism of this type of structure. With the goal of theoretical investigation, pure friction systems have been employed extensively in the past [61,62]. The novelties of the paper compared to previous studies [5,57,58] are employment of the inerter technique for performance improvement of sliding isolation structures, analytical solutions for the dynamic responses and explicit expressions for conditions of motion modes of inerter-added sliding isolation structures that assist in understanding the role of the additional inerter.

In this study, closed-form solutions for the dynamic characteristics and responses of inerter-added sliding isolation structures are derived. The explicit expressions for the occurrence conditions of the three

fundamental motion modes (i.e., the stick-stick mode, the stick-slip mode and slip-slip mode reported in [63]) of the pure friction system with an additional inerter are derived based on the steady-state response. Numerical analyses are conducted to validate the explicit expressions. According to the derivations presented above, the influences of the added inerter on the motion mode, the maximum acceleration of the superstructure and the amplitude of the isolation displacement of the pure-friction isolation structure are investigated.

This paper is structured as follows. Section 2 presents the governing equations of motion for both the stick and sliding phases of the inerter-added sliding isolation structures. Then, the corresponding analytical solutions of the structural responses are provided. In Section 3, the conditions of the three fundamental motion modes of the inerter-added sliding isolation structures are derived and verification studies are performed. Section 4 gives parametric analyses of the dynamic responses of the inerter-added sliding isolation structures. Conclusions are presented at the end of this paper.

2. Theoretical basis

To facilitate analytical solutions of the inerter-added sliding isolation structure, an appropriate mechanical model needs to be built to illustrate its dynamic behavior. The governing equations of motion for the inerter-added sliding isolation structure are derived under ground motion excitations using an appropriate mechanical model in this section. By solving the governing equations of motion, explicit expressions for the dynamic responses of the structure are obtained. Then, based on the structural dynamic responses, the characteristics for motions of the inerter-added sliding isolation structure are illustrated. The details of this section are given below.

2.1. Governing equations of motion

Fig. 1 shows the mechanical model of the inerter-added sliding isolation structure. The pure-friction system with an additional inerter is incorporated between the isolated base and the ground. The superstructure is simplified as a single degree of freedom (SDOF) system, which is commonly used as an equivalent of an isolated object [24,53]. Note that for the whole system, the inerter-added sliding isolation structure is a two-degrees-of-freedom system. This can also be seen from the derivation of equations of motion for the whole structure below. The additional inerter employed here is to improve the performance of the sliding isolation structure, such as the displacement performance of the isolation layer. Due to the apparent mass effect, the inerter can realize the performance adjustment of the sliding isolation structure with a quite small gravitational mass that can be ignored.

In Fig. 1, m, c and k denote the mass, damping coefficient and stiffness of the superstructure, respectively; m_b is the mass of the isolated base; x_s denotes the relative displacement between the primary mass and the isolated base, and y_b denotes the relative displacement between the isolated base and the ground; x, y and z are the absolute displacements of the primary mass, the isolated base and the ground, respectively; and m_{in} is referred to as the inertance (also called apparent mass) of the inerter. The inerter is a recently developed two-terminal inertial element whose output force is proportional to the relative acceleration of its two ends. Assuming that the accelerations of the two ends of the inerter are $\ddot{x}_1$ and $\ddot{x}_2$, as shown in Fig. 2, the output force F_{in} of the inerter can be written as

$$F_{in} = m_{in}\left(\ddot{x}_2 - \ddot{x}_1\right) \tag{1}$$

In addition, the relationships between displacements expressed in Fig. 1 are as follows:

$$x = z + y_b + x_s \tag{2}$$

$$y = z + y_b \tag{3}$$

According to the dynamic equilibrium approach, the governing equations of motion for the inerter-added sliding isolation structure under ground motion excitations can be expressed as follows:

$$\begin{cases} m\ddot{x} + c\dot{x}_s + kx_s = 0 \\ m_b\ddot{y} + m_{in}\ddot{y}_b + m\ddot{x} = f \end{cases} \tag{4}$$

where f is the friction force along the sliding interfaces between the isolated base and the ground. The first equation of Eq. (4) is the dynamic equilibrium of the superstructure, whereas the second equation can be seen as the dynamic equilibrium of the isolated base. The ideal Coulomb model is adopted here to describe the friction force, which is simple and appropriate for the derivation of analytical solutions. The mechanical behavior of the ideal Coulomb model is shown in Fig. 3. The friction force f can be expressed as

$$|f| \le \mu(m + m_b)g \tag{5}$$

where μ is the friction coefficient, and g denotes the acceleration of gravity.

The condition of the stick motion of the inerter-added sliding isolation structure is as follows: (1) the absolute value of f is no more than $\mu(m + m_b)g$, and (2) the sliding velocity $\dot{y}$ and the sliding acceleration $\ddot{y}$ are equal to the velocity $\dot{z}$ and the acceleration $\ddot{z}$ of ground motions, respectively. When sliding occurs, the friction force f is calculated as

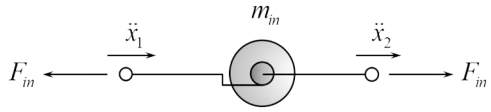

Fig. 2. Mechanical model of the two-terminal inerter.

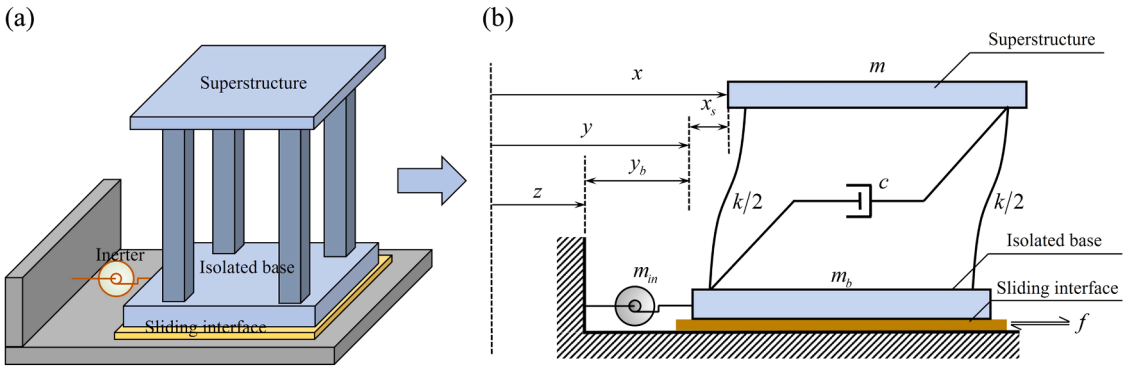

Fig. 1. Modeling of the inerter-added sliding isolation structure, where an inerter is employed at the base isolation layer for performance improvement: (a) Three-dimensional representation and (b) two-dimensional representation with key parameters.

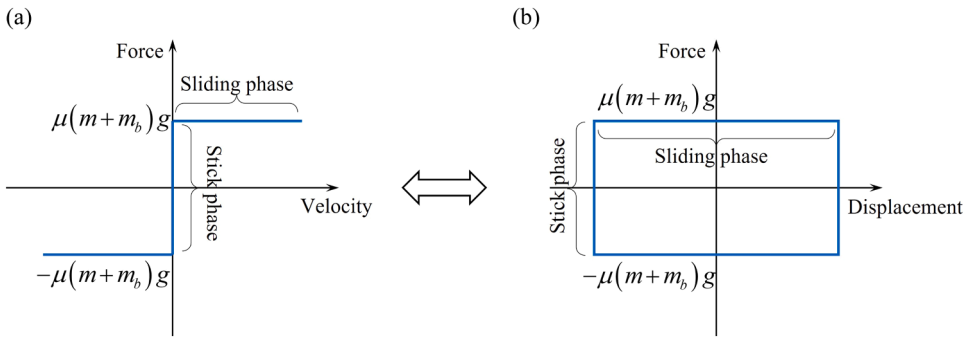

Fig. 3. Mechanical behavior of the Coulomb model representing motions between sliding interfaces of inerter-added sliding isolation structures, where the sliding and stick motion states are indicated: (a) Force versus velocity and (b) force versus displacement.

$$f = \mu(m+m_b)g\cdot\mathrm{sgn}(\dot{z}-\dot{y}) \tag{6}$$

where sgn (•) is the signum function. Based on friction forces during the stick and sliding motion phases illustrated above, the governing equations of motion for these two phases can be derived as follows.

(i) *During the stick phases*, the corresponding governing equations of motion expressed as Eq. (4) can be written with a dimensionless form as

$$\begin{cases} \ddot{x}_s + 2\zeta_0\omega_0\dot{x}_s + \omega_0^2 x_s = -\ddot{z} \\ \alpha\ddot{x}_s + \ddot{z} = f/(m+m_b), \text{where} |f| \le \mu(m+m_b)g \end{cases} \tag{7}$$

where ω_0 and ζ_0 are the natural frequency and damping ratio of the superstructure, respectively, and α is the ratio of the mass of superstructure to the total mass. They are expressed as

$$\omega_0 = \frac{k}{m}, \zeta_0 = \frac{c}{2m\omega_0}, \alpha = \frac{m}{m+m_b} \tag{8}$$

Combining the two expressions in the second equation of Eq. (7) gives

$$\left|\alpha\ddot{x}_s + \ddot{z}\right| \le \mu g \tag{9}$$

Eq. (9) is the condition of the stick phases of the inerter-added sliding isolation structure. When contrary to this condition, sliding motion starts.

(ii) *During the slippage phases*, the corresponding governing equations of motion can be written with a dimensionless form by substituting Eq. (6) and the relationships of the displacements expressed in Eqs. (2) and (3) into Eq. (4) as

$$\begin{cases} \ddot{x}_s + 2\zeta_1\omega_1\dot{x}_s + \omega_1^2 x_s = -\dfrac{\mu g}{1+\beta-\alpha}\cdot\mathrm{sgn}(\dot{z}-\dot{y}) - \dfrac{\beta}{1+\beta-\alpha}\ddot{z} \\ \ddot{y} = \mu\dfrac{1}{1+\beta}g\cdot\mathrm{sgn}(\dot{z}-\dot{y}) - \dfrac{\alpha}{1+\beta}\ddot{x}_s + \dfrac{\beta}{1+\beta}\ddot{z} \end{cases} \tag{10}$$

where β denotes the ratio of the inertance to the total mass and ω_1 and ζ_1 are the natural frequency and the damping ratio of the superstructure during slippage phases, respectively. They can be expressed as

$$\beta = \frac{m_{in}}{m+m_b}, \omega_1 = \omega_0\sqrt{\frac{1+\beta}{1+\beta-\alpha}}, \zeta_1 = \zeta_0\sqrt{\frac{1+\beta}{1+\beta-\alpha}} \tag{11}$$

Since the time of initiation of the slippage phase is infinitesimally close to the time of the end of the stick phase, the condition for initiation of slippage can be expressed as

$$\left|\alpha\ddot{x}_s + \ddot{z}\right| \ge \mu g \tag{12}$$

The condition for reattachment of the isolated base and the ground is written as

$$\dot{y} = \dot{z}, \text{and} \left|\alpha\ddot{x}_s + \ddot{z}\right| \le \mu g \tag{13}$$

Note that the dimensionless mathematical framework adopted in Eqs. (7) and (10) can substantially reduce the number and complexity of the fundamental parameters required for describing the responses of the whole system. The parametric analyses illustrated in Section 5 can also be conducted more conveniently.

Based on the derivations above, it can be seen that during the stick phases, the governing equation of motion for the superstructure in an inerter-added sliding isolation structure is equivalent to that of a fixed base SDOF structure subjected to ground motions. Hence, it is said that the inerter does not function in stick phases. This is consistent with the working mechanism of the inerter that a nonzero relative acceleration should exist between its two ends. Meanwhile, adding an inerter has no impact on the condition for the stick phases, as described in Eq. (9).

During the slippage phases, the vibration of the superstructure behaves with an adjusted frequency of ω_1 and an adjusted damping ratio of ζ_1, which are related to the values of α and β, as shown in the first equation of Eq. (10). In addition, the corresponding excitation for the vibration of the superstructure shows a combination of a step force and a reduced ground motion. As a result, the responses of the structure are altered due to the additional inerter. When β = 0 (i.e., the inerter is not added at the sliding isolation structure), Eq. (10) can be degraded to the governing equations of motion of a sliding isolation structure without an inerter. For this isolation structure, the natural frequency and damping ratio of the superstructure during slippage phases have been derived as $\omega_0\sqrt{1/(1-\alpha)}$ and $\zeta_0\sqrt{1/(1-\alpha)}$, respectively, in [56]. These can also be obtained by substituting β = 0 into Eq. (11) in this study. Since the value of α is less than 1 and β is nonnegative, the value of $\sqrt{(1+\beta)/(1+\beta-\alpha)}$ is less than the value of $\sqrt{1/(1-\alpha)}$. Hence, adding an inerter can decrease the frequency and damping ratio of the sliding isolation structure during the slippage phase.

2.2. Responses of inerter-added sliding isolation structures

According to the governing equations of motion of the inerter-added sliding isolation structure illustrated above, the analytical solutions for the stick and slippage phases under harmonic ground excitations are discussed here. During the stick phases, the first equation of Eq. (7) is equivalent to the governing equation of an SDOF structure under ground motion excitations. The analytical solutions for such a structure have been addressed in the textbook on dynamics of structures. During the slippage phases, the first equation of Eq. (10) is the governing equation of an SDOF structure with a frequency of ω_1 and damping ratio of ζ_1 subjected to the combination of a step force and a reduced ground motion excitation. Assuming the external excitation is written as $\ddot{z} = a_0\sin\omega t$, where a_0 and ω are the amplitude and frequency of the ground motion, respectively, the solution of this equation can be expressed as

$$\begin{bmatrix} x_s(t) \\ \dot{x}_s(t) \end{bmatrix} = \mathbf{A}_s(\tau)\begin{bmatrix} x_s(t_i) \\ \dot{x}_s(t_i) \end{bmatrix} + \mathbf{B}_s(\tau) \tag{14}$$

where t denotes the global time for the structural responses, t_i is the moment when sliding starts in the ith slippage phase, $\tau = t - t_i$ is the local time, and

$$\mathbf{A}_s(\tau) = e^{-\zeta_1\omega_1\tau}\begin{bmatrix} \cos(\omega_{1d}\tau) + \dfrac{\zeta_1}{\sqrt{1-\zeta_1^2}}\sin(\omega_{1d}\tau) & \dfrac{1}{\omega_1\sqrt{1-\zeta_1^2}}\sin(\omega_{1d}\tau) \\ -\dfrac{\omega_1}{\sqrt{1-\zeta_1^2}}\sin(\omega_{1d}\tau) & \cos(\omega_{1d}\tau) - \dfrac{\zeta_1}{\sqrt{1-\zeta_1^2}}\sin(\omega_{1d}\tau) \end{bmatrix} \tag{15}$$

$$\mathbf{B}_s(\tau) = \mathbf{B}_{s,1}(\tau) + \mathbf{B}_{s,2}(\tau) \tag{16}$$

$$\mathbf{B}_{s,1}(\tau) = \frac{\mu g}{\omega_1^2(1+\beta-\alpha)}\cdot\mathrm{sgn}(\dot{z}-\dot{y})\begin{bmatrix} e^{-\zeta_1\omega_1\tau}\left(\dfrac{\zeta_1}{\sqrt{1-\zeta_1^2}}\sin\omega_{1d}\tau + \cos\omega_{1d}\tau\right) - 1 \\ -\dfrac{\omega_1}{\sqrt{1-\zeta_1^2}}e^{-\zeta_1\omega_1\tau}\sin\omega_{1d}\tau \end{bmatrix} \tag{17}$$

$$\mathbf{B}_{s,2}(\tau) = \frac{\beta a_0}{(1+\beta-\alpha)\omega_1^2}\begin{bmatrix} e^{-\zeta_1\omega_1\tau}\left[-q\left(\dfrac{\zeta_1}{\sqrt{1-\zeta_1^2}}\sin(\omega_{1d}\tau) + \cos(\omega_{1d}\tau)\right) - \dfrac{p\omega}{\omega_{1d}}\sin(\omega_{1d}\tau)\right] + p\sin(\omega\tau) + q\cos(\omega\tau) \\ e^{-\zeta_1\omega_1\tau}\left[\dfrac{q\omega_1}{\sqrt{1-\zeta_1^2}}\sin(\omega_{1d}\tau) + p\omega\left(\dfrac{\zeta_1}{\sqrt{1-\zeta_1^2}}\sin(\omega_{1d}\tau) - \cos(\omega_{1d}\tau)\right)\right] + p\omega\cos(\omega\tau) - q\omega\sin(\omega\tau) \end{bmatrix} \tag{18}$$

$$\omega_{1d} = \omega_1\sqrt{1-\zeta_1^2} \tag{19}$$

$$p = -\frac{\left(1-\frac{\omega^2}{\omega_1^2}\right)\cos\omega t_i + 2\zeta_1\frac{\omega}{\omega_1}\sin\omega t_i}{\left(1-\frac{\omega^2}{\omega_1^2}\right)^2 + \left(2\zeta_1\frac{\omega}{\omega_1}\right)^2} \tag{20}$$

$$q = -\frac{\left(1-\frac{\omega^2}{\omega_1^2}\right)\sin\omega t_i - 2\zeta_1\frac{\omega}{\omega_1}\cos\omega t_i}{\left(1-\frac{\omega^2}{\omega_1^2}\right)^2 + \left(2\zeta_1\frac{\omega}{\omega_1}\right)^2} \tag{21}$$

For the solution expressed by Eq. (14), the first term on the right-hand side involves the free vibration of the corresponding structure with initial conditions, whereas the second term involves the vibration induced by a step force and a reduced ground motion excitation that are further expressed by Eq. (17) and Eq. (18), respectively. When $\beta = 0$, Eq. (14) is equivalent to solutions of the superstructure of the sliding isolation structure without an inerter.

By integrating the second equation of Eq. (10) once and determining the initial velocity of the isolated base $\dot{y}(t_i)$ in the ith slippage phase (equal to $\dot{z}(t_i)$), the velocity $y(t)$ is calculated as

$$\dot{y}(t) = \mu\frac{1}{1+\beta}g\cdot\mathrm{sgn}(\dot{z}-\dot{y})\tau - \frac{\alpha}{1+\beta}(\dot{x}_s(t)-\dot{x}_s(t_i)) + \frac{\beta}{1+\beta}(\dot{z}(t)-\dot{z}(t_i)) + \dot{y}(t_i) \tag{22}$$

Then, Eq. (22) is integrated again to obtain the displacement of the isolated base $y(t)$, written as

$$y(t) = \frac{1}{2}\mu\frac{1}{1+\beta}g\cdot\mathrm{sgn}(\dot{z}-\dot{y})\tau^2 - \frac{\alpha}{1+\beta}(x_s(t)-x_s(t_i)-\dot{x}_s(t_i)\tau) + \frac{\beta}{1+\beta}(z(t)-z(t_i)-\dot{z}(t_i)\tau) + \dot{y}(t_i)\tau + y(t_i) \tag{23}$$

where $y(t_i)$ denotes the displacement of the isolated base at time t_i.

The ith slippage phase stops when the velocity $y(t)$ in this phase is equal to the velocity of the ground $\dot{z}(t)$ again. When this round of the slippage phase ends, the inerter-added sliding isolation structure may continue to slip or change to stick, which is determined by the condition of Eq. (13).The solutions derived above in slippage phases show that the parameter of the inerter can impact the responses of the sliding isolation structure, and therefore the condition of the moment when the ith slippage phase stops (determined by Eq. (13)).

2.3. Illustration of three motion modes of sliding isolation structures

It has been demonstrated that the motion of the sliding isolation structure has three different modes: the stick-stick mode, the stick-slip mode and the slip-slip mode [63]. In the stick-stick mode of a sliding isolation structure, only stick motion phases occur. This mode usually occurs for a sliding isolation structure under ground excitation with a small amplitude. In contrast, in the slip-slip mode, only slip motion phases occur for a sliding isolation structure, and this mode occurs under ground excitation with large amplitude. When both the stick and slip phases occur in one whole motion period, the motion mode of the sliding isolation structure is called the stick-slip mode. Since the additional inerter proposed in this study adjusts the dynamic characteristics of the sliding isolation structure and thus improves the performance of this structure, the inherent working mechanism of the sliding isolation system remains unchanged. Hence, these three motion modes also exist at the inerter-added sliding isolation structure. Compared to the stick-slip mode, the slip-slip mode is preferred for the motion of the sliding isolation structure based on the characteristics of the structural responses [7,61]. For a more comprehensive understanding, we give an overview in detail about these three motion modes herein.

Previous studies found that the periodic motions will be observed in steady-state responses of sliding isolation structures subjected to harmonic excitations [56]. Fig. 4 shows the schematic velocity and acceleration of the isolated base and ground in one cycle for the steady-state responses of the inerter-added sliding isolation structure with the same period of ground motion excitations. Note that the curves shown in Fig. 4 are presented qualitatively and obtained based on the derivations in Section 2.2 for a certain case, where t_0 is the start moment of the stick motion, t_i is the end of this stick motion as well as the start of slip motion, and t_f is the end of this slip motion. The motion of the inerter-added sliding isolation structure in Fig. 4(b) includes both the stick and slip motions, which is the so-called stick-slip mode. When the moment t_i coincides with t_0, the stick-slip mode is transformed into the slip-slip mode (see Fig. 4(c)). Only slip motion phases exist in the slip-slip mode of the structure. In contrast, the stick-stick mode occurs when the moment t_i coincides with t_f, which only includes the stick motion for

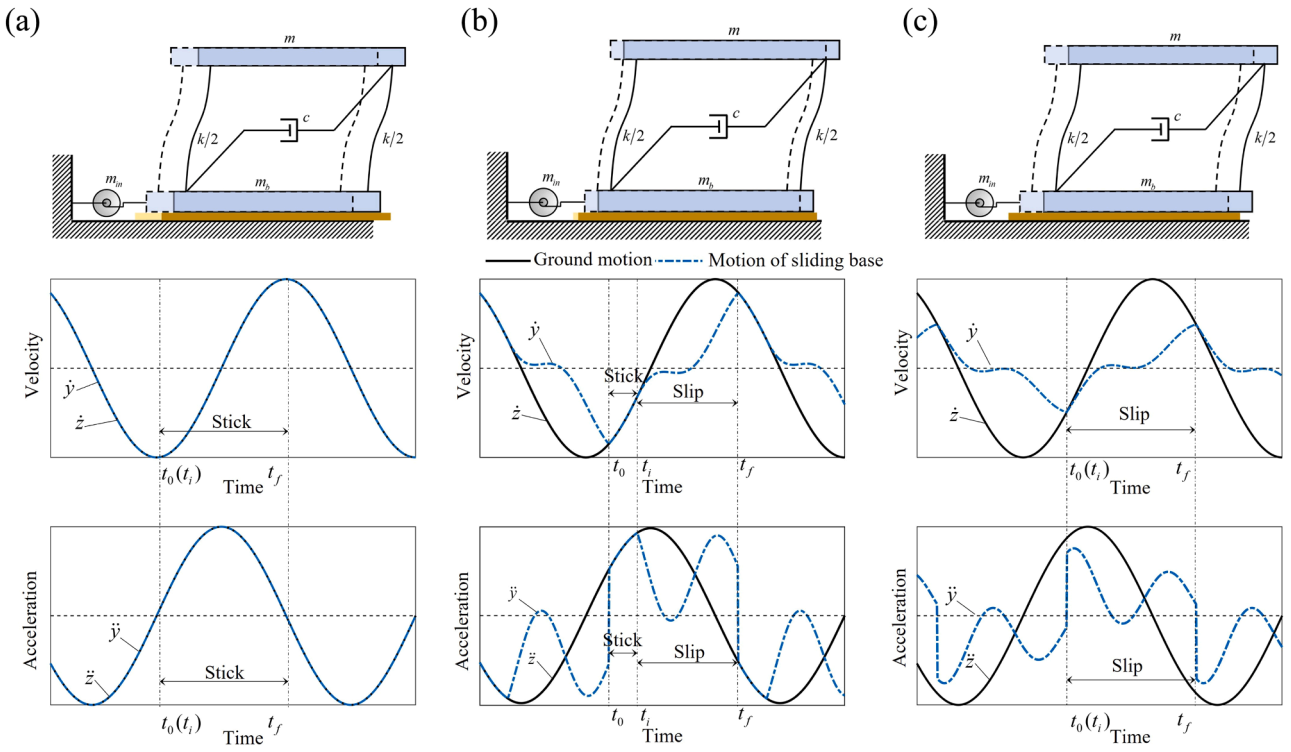

Fig. 4. Schematic representation of the velocity and acceleration responses of the isolated base and ground in an inerter-added sliding isolation structure with different motion modes: (a) Stick-stick mode, (b) stick-slip mode, and (c) slip-slip mode.

the inerter-added sliding isolation structure (see Fig. 4(a)).

Based on the derivations in Section 2.2, several time history responses are presented in Figs. 5 and 6 to show the motions of inerter-added sliding isolation structures with stick-slip and slip-slip modes, respectively, which can provide a visual demonstration of the illustrations above and some basis for the investigations of the following sections. The initial displacement and velocity of the structure are set as zero. The parameters of the inerter-added sliding isolation structure in Fig. 5 are $\mu = 0.1$, $T_0 = 2\pi/\omega_0 = 0.5$s, $\zeta_0 = 0.05$, $\alpha = 0.5$, $\beta = 0.1$, $a_0 = 0.2g$ and $T = 2\pi/\omega = 1$s, where T_0 and T are the periods of the superstructure and the ground motion, respectively. The absolute acceleration of the superstructure $\ddot{x}$ (related to the base shear force) and the displacement of the isolation layer y_b are selected to be exhibited here, which are concerned with the performances of isolation structures. An extensive investigation of these two responses is also performed to evaluate the performances of inerter-added sliding isolation structures in Section 4. Fig. 5 shows that the responses of the structure converge to steady state after several motion cycles whose period is the same as the harmonic ground motion. Each cycle of the steady-state response contains two stick and slip motion intervals. For the two slip motion intervals in one cycle, the structure slides in opposite directions. Under a certain excitation frequency, the motion of a certain isolation structure with the stick-slip mode will transfer into the motion of the slip-slip mode when the amplitude of the excitation exceeds the threshold value. Under an increased ground motion amplitude of 1.2g, the responses for the motion of the slip-slip mode are shown in Fig. 6 for the inerter-added sliding isolation structure with the same parameters as those in Fig. 5. There are no stick phases, and the sliding direction changes after a slippage phase ends in one cycle. In Figs. 5 and 6, $y_{b,ap}$ denotes the amplitude of the displacement of the isolation layer during the steady-state response, which is adopted as an index to evaluate the performance of the inerter-added sliding isolation structure involving the isolation displacement in the section below. Under harmonic ground motion excitations, the maximum isolation displacements accumulate due to the transient responses before the periodic steady-state motion. Hence, the maximum isolation displacements are strongly dependent on the initial acceleration of the ground excitation. Consequently, the amplitude of the isolation displacement, $y_{b,ap}$, rather than its maximum value, is selected as the evaluation index. When the acceleration of the ground motion is small enough, the stick-stick mode occurs for the motion of the isolation structure. Since the responses of the inerter-added sliding isolation structure in this mode are the same as those of the familiar fixed base structure, it is not shown here.

3. Occurrence conditions for three motion modes

The explicit expressions for the occurrence conditions of the three modes illustrated above are derived in this section based on steady-state responses of inerter-added sliding isolation structures. Using these derived explicit expressions, numerical integration will not be necessary for determining the mode of the inerter-added sliding isolation structure. Since the motion and condition of the sliding isolation structure is not impacted by the additional inerter during stick phases, the boundary between the stick-stick mode and the stick-slip mode is the same for the sliding isolation structure with inerter and without inerter, which has been derived in [56]. This is also verified by the numerical analysis exhibited at the end of this section. Hence, only the boundary that separates the regions of the stick-slip mode and the slip-slip mode is derived in detail here.

Based on the derivations in Section 2.1 for sliding phases of the inerter-added sliding isolation structure, the first equation of Eq. (10) is equivalent to the governing equation of an SDOF structure with frequency ω_1 and damping ratio ζ_1 subjected to the combination of a step force and a reduced ground motion excitation. For one cycle of periodic motion in slip-slip mode, the structure slides in one direction for half of the period of the ground motion and then in the opposite direction for the other half of the period, as shown in Fig. 6. Assuming the harmonic ground motion, the combining excitation in the first half of one cycle has the same absolute values but contrary signs with that of the other half cycle, so are the steady-state solutions of the first equation of Eq. (10) for

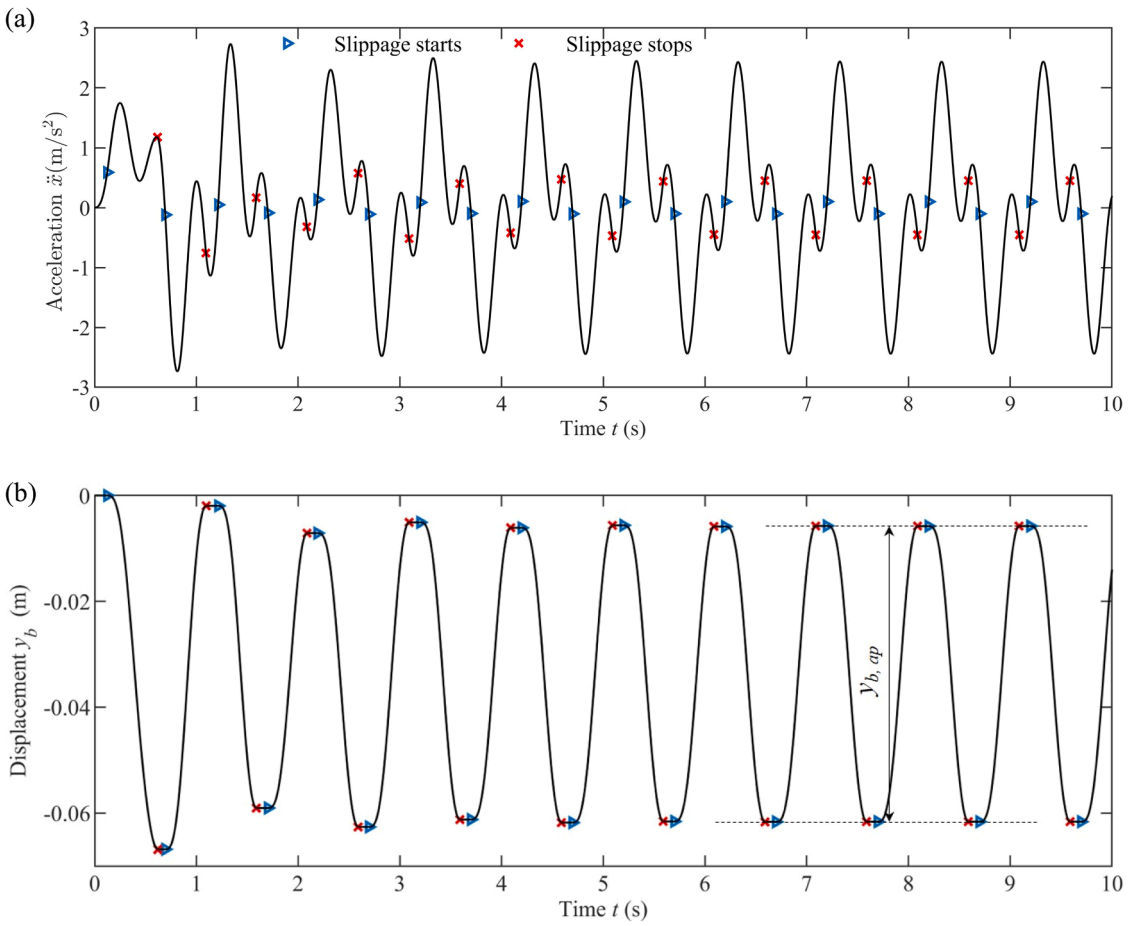

Fig. 5. Responses of an inerter-added sliding isolation structure behaving in stick-slip motion mode, computed for μ = 0.1, T_0 = 0.5s, ζ_0 = 0.05, α = 0.5, β = 0.1, $T = 2\pi/\omega$ = 1s and a_0 = 0.2g, where the closed-form solutions during different motion states are employed: (a) Acceleration time history response and (b) displacement time history response.

the two half cycles. At the beginning of the slip-slip mode, the time interval between t_i (which coincides with t_0) and t_f is equal to π/ω (i.e., $t_f - t_i = \pi/\omega$). Taking into account the relationships of the solutions above, letting $t = t_f$ and substituting $t_f - t_i = \pi/\omega$ into Eq. (14), this equation can be rewritten as

$$\begin{bmatrix} x_s(t_f) \\ \dot{x}_s(t_f) \end{bmatrix} = \mathbf{A}_s\left(\frac{\pi}{\omega}\right)\begin{bmatrix} x_s(t_i) \\ \dot{x}_s(t_i) \end{bmatrix} + \mathbf{B}_s\left(\frac{\pi}{\omega}\right) = -\begin{bmatrix} x_s(t_i) \\ \dot{x}_s(t_i) \end{bmatrix} \tag{24}$$

Following Eq. (24), the displacement $x_s(t_i)$ and the velocity $\dot{x}_s(t_i)$ can be calculated as follows:

$$\begin{bmatrix} x_s(t_i) \\ \dot{x}_s(t_i) \end{bmatrix} = -\left[\mathbf{A}_s\left(\frac{\pi}{\omega}\right) + \mathbf{I}\right]^{-1}\mathbf{B}_s\left(\frac{\pi}{\omega}\right) \tag{25}$$

where denotes the identity matrix. Based on the expressions of $\mathbf{A}_s(\tau)$ and $\mathbf{B}_s(\tau)$ in Eqs. (15)–(21), $x_s(t_i)$ and $\dot{x}_s(t_i)$ can be expressed as

$$x_s(t_i) = \frac{\beta a_0}{(1+\beta)\omega_0^2}q + \frac{\mu g \mathrm{sgn}(\dot{z}-\dot{y})}{(1+\beta)\omega_0^2}\cdot\frac{\sinh\varphi - \sin\psi\frac{\zeta_1}{\sqrt{1-\zeta_1^2}}}{\cosh\varphi + \cos\psi} \tag{26}$$

$$\dot{x}_s(t_i) = \frac{\beta a_0 \omega}{(1+\beta)\omega_0^2}p + \frac{\mu g \mathrm{sgn}(\dot{z}-\dot{y})}{(1+\beta)\omega_0^2}\cdot\frac{\sin\psi}{\cosh\varphi + \cos\psi}\cdot\frac{\omega_1}{\sqrt{1-\zeta_1^2}} \tag{27}$$

where p and q are defined in Eqs. (20) and (21), respectively, and

$$\varphi = \frac{\pi\zeta_1\omega_1}{\omega}, \psi = \frac{\pi\omega_{1d}}{\omega} \tag{28}$$

At the initiation of the slippage phase (i.e., $t = t_i$), the condition expressed by Eq. (12) is satisfied and written as

$$\left|\alpha\ddot{x}_s + \ddot{z}\right| = \left|\alpha\left[-2\zeta_0\omega_0\dot{x}_s(t_i) - \omega_0^2 x_s(t_i) - a_0\sin(\omega t_i)\right] + a_0\sin(\omega t_i)\right| \geq \mu g \tag{29}$$

Substituting Eqs. (26) and (27) into Eq. (29), this inequality can be expressed as follows through a rearrangement:

$$\left|(1+\beta-\alpha)[\gamma_1\sin(\omega t_i) - \gamma_2\cos(\omega t_i)]\cdot\frac{a_0}{\mu g} - \frac{\alpha\mathrm{sgn}(\dot{z}-\dot{y})}{1+\beta}\cdot\frac{\sin\psi\frac{\zeta_1}{\sqrt{1-\zeta_1^2}} + \sinh\varphi}{\cos\psi + \cosh\varphi}\right| \geq 1 \tag{30}$$

where

$$\gamma_1 = \frac{\frac{4\omega^2\zeta_1^2}{\omega_1^2} + \left(1-\frac{\omega^2}{\omega_1^2}\right)\left(1+(\alpha-1)\frac{\omega^2}{\omega_0^2}\right)}{\left[\left(1-\frac{\omega^2}{\omega_1^2}\right)^2 + \left(\frac{2\omega\zeta_1}{\omega_1}\right)^2\right](1+\beta)} \tag{31}$$

$$\gamma_2 = \frac{\frac{2\alpha\beta\zeta_0\omega^3}{(1+\beta)\omega_0^3}}{\left[\left(1-\frac{\omega^2}{\omega_1^2}\right)^2 + \left(\frac{2\omega\zeta_1}{\omega_1}\right)^2\right](1+\beta)} \tag{32}$$

At the beginning of the slippage phase, the sign of $(\dot{z} - \dot{y})$ is determined by

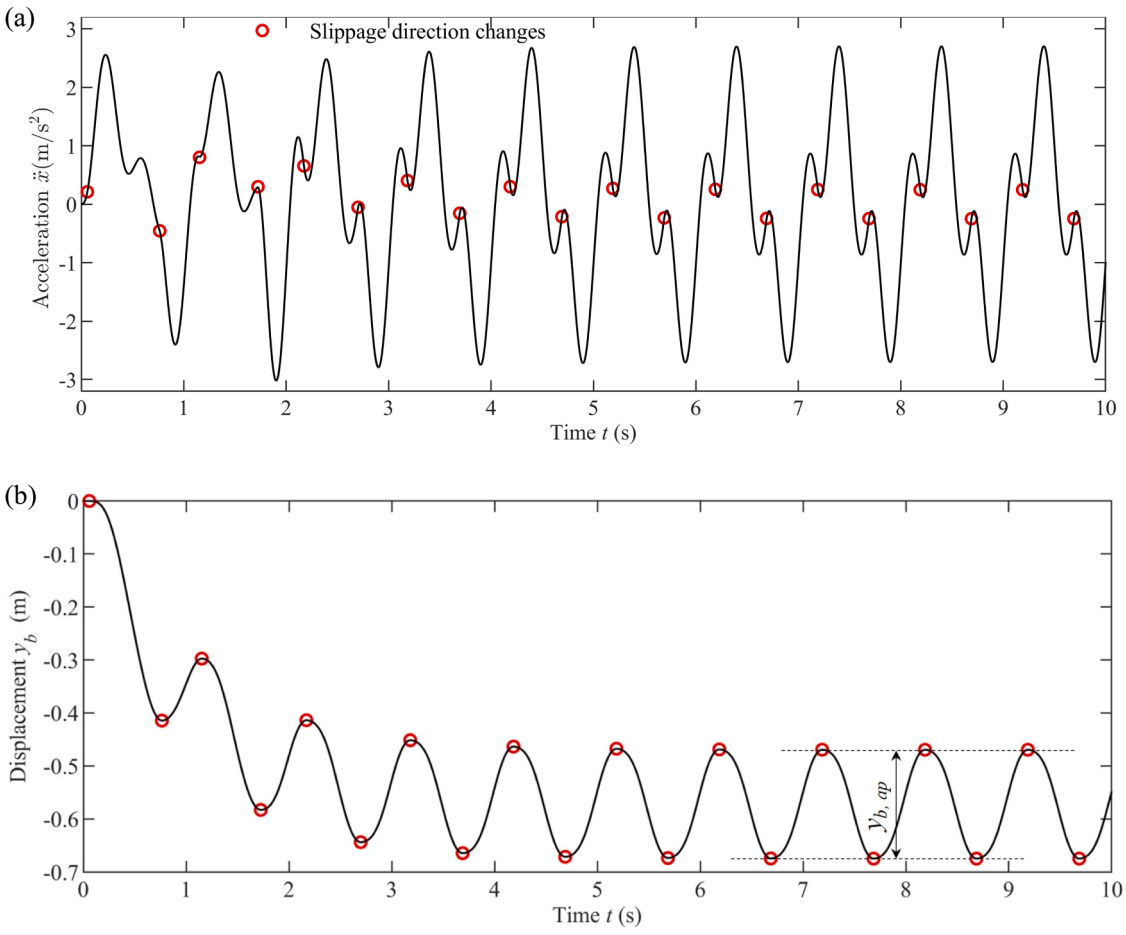

Fig. 6. Responses of an inerter-added sliding isolation structure behaving in slip-slip motion mode, computed for $\mu = 0.1$, $T_0 = 0.5$s, $\zeta_0 = 0.05$, $\alpha = 0.5$, $\beta = 0.1$, $T = 2\pi/\omega = 1$s and $a_0 = 1.2$g, where the closed-form solutions during different motion states are employed: (a) Acceleration time history response and (b) displacement time history response.

$$\mathrm{sgn}(\dot{z}-\dot{y}) = \frac{\alpha\ddot{x}_s + \ddot{z}}{\left|\alpha\ddot{x}_s + \ddot{z}\right|} \tag{33}$$

Then, considering that the expression in the sign of the absolute value of Eq. (30) is the variant of $(\alpha\ddot{x}_s + \ddot{z})/\mu g$, Eq. (30) can be rewritten with the help of Eq. (33) as follows:

$$[\gamma_1 \sin(\omega t_i) - \gamma_2 \cos(\omega t_i)]^2 \cdot \left|\frac{a_0}{\mu g}\right|^2 \geq F_0^2 \tag{34}$$

where

$$F_0^2 = \frac{1}{(1+\beta-\alpha)^2}\left(1 + \frac{\alpha}{1+\beta}\cdot\frac{\sin\psi\frac{\zeta_1}{\sqrt{1-\zeta_1^2}} + \sinh\varphi}{\cos\psi + \cosh\varphi}\right)^2 \tag{35}$$

In addition, at the moment that the stick-slip mode switches to the slip-slip mode, the velocity of the isolated base equals that of the ground motion. This is expressed as follows at time $t = t_i$:

$$\dot{y}(t_i) = \dot{z}(t_i) \tag{36}$$

According to the periodic characteristics of the solutions in the slip-slip mode, we have

$$\dot{y}(t_f) = -\dot{y}(t_i) \tag{37}$$

In a half cycle of the steady-state motion of the structure with slip-slip mode, letting $t = t_f$, $\tau = t_f - t_i = \pi/\omega$ and considering the relations in Eqs. (36) and (37), Eq. (22) can be rewritten as

$$\frac{2a_0}{\omega}\cos(\omega t_i) = \mu g \cdot \mathrm{sgn}(\dot{z}-\dot{y})\frac{\pi}{\omega} + 2\alpha\dot{x}_s(t_i) \tag{38}$$

Substituting Eq. (27) into Eq. (38) yields

$$\frac{2a_0}{\omega}\left[\cos(\omega t_i) - \frac{\alpha\beta\omega^2}{(1+\beta)\omega_0^2}p\right] = \left[\mu g\cdot\left(\frac{\pi}{\omega} + \frac{2\alpha}{(1+\beta)\omega_0^2}\frac{\sin\psi}{\cosh\varphi+\cos\psi}\cdot\frac{\omega_1}{\sqrt{1-\zeta_1^2}}\right)\right]\cdot\mathrm{sgn}(\dot{z}-\dot{y}) \tag{39}$$

Eq. (39) can be expressed as follows through a rearrangement:

$$\frac{a_0}{\mu g}[\gamma_1 \cos(\omega t_i) + \gamma_2 \sin(\omega t_i)] = \gamma_3 \tag{40}$$

where

$$\gamma_3 = \left[\frac{1}{1+\beta}\left(\frac{\pi}{2} + \frac{\alpha\omega}{(1+\beta)\omega_0}\frac{\sin\psi}{\cosh\varphi + \cos\psi}\frac{\omega_1}{\omega_0\sqrt{1-\zeta_1^2}}\right)\right]\cdot \mathrm{sgn}(\dot{z} - \dot{y}) \tag{41}$$

Combining Eq. (34) and the square of Eq. (40), it is derived by eliminating the harmonic terms of $\sin(\omega t_i)$ and $\cos(\omega t_i)$ as

$$\left|\frac{a_0}{\mu g}\right| \geq \sqrt{\frac{1}{\gamma_1^2 + \gamma_2^2}}\cdot\sqrt{\gamma_3^2 + F_0^2} \tag{42}$$

Eq. (42) is the explicit form of the occurrence condition of the slip-slip mode for inerter-added sliding isolation structures. The explicit expressions of the conditions of the stick-stick mode are the same for the sliding isolation structure with an inerter and without an inerter according to the corresponding governing equations of motion, which have been derived by Westermo and Udwadia [56]. Consequently, the expressions for the conditions of the three modes of the inerter-added sliding isolation structure can be summarized as follows:

(1) Conditions of the stick-stick mode

$$\left|\frac{a_0}{\mu g}\right| \leq \sqrt{\frac{1}{(\gamma_4 + 1)^2 + \gamma_5^2}} \tag{43}$$

(2) Conditions of the stick-slip mode

$$\sqrt{\frac{1}{\gamma_1^2 + \gamma_2^2}}\cdot\sqrt{\gamma_3^2 + F_0^2} \leq \left|\frac{a_0}{\mu g}\right| \leq \sqrt{\frac{1}{(\gamma_4 + 1)^2 + \gamma_5^2}} \tag{44}$$

(3) Conditions of the slip-slip mode

$$\left|\frac{a_0}{\mu g}\right| \geq \sqrt{\frac{1}{\gamma_1^2 + \gamma_2^2}}\cdot\sqrt{\gamma_3^2 + F_0^2} \tag{45}$$

where

$$\gamma_4 = \frac{\alpha\frac{\omega^2}{\omega_0^2}\left(1 - \frac{\omega^2}{\omega_0^2}\right)}{\left(1 - \frac{\omega^2}{\omega_0^2}\right)^2 + \left(\frac{2\omega\zeta_0}{\omega_0}\right)^2} \tag{46}$$

$$\gamma_5 = \frac{-2\frac{\omega^3}{\omega_0^3}\zeta_0\alpha}{\left(1 - \frac{\omega^2}{\omega_0^2}\right)^2 + \left(\frac{2\omega\zeta_0}{\omega_0}\right)^2} \tag{47}$$

When $\beta = 0$, Eqs. (44) and (45) agree with the corresponding derivations given by Iura et al. [63] for the sliding isolation structure without an inerter. To verify the explicit forms for the conditions of the three modes in Eqs. (43)–(45), these analytical results are compared with the numerical results for two inerter-added sliding isolation structures with different parameters. The boundaries between the three modes are depicted through relationships between the frequency ratios ω/ω_0 and normalized accelerations $a_0/\mu g$, as shown in Fig. 7. Using the solid boundary line obtained by Eqs. (43)–(45), the regions for the three modes of inerter-added sliding isolation structures are clearly separated. The numerical results obtained using the solutions in Section 2 are shown in Fig. 7 with a scatter plot for several frequency ratios. Fig. 7(a) is obtained for structures with parameters of $\zeta_0 = 0.05$, $\alpha = 0.2$ and $\beta = 0.2$, and the corresponding parameters for Fig. 7(b) are $\zeta_0 = 0.05$, $\alpha = 0.5$ and $\beta = 0.4$. The theoretical and numerical results show good agreement in both figures. Hence, the derived explicit expressions of occurrence conditions are verified. The boundaries represented by the normalized excitation amplitude $a_0/\mu g$ in Fig. 7(b) are generally larger

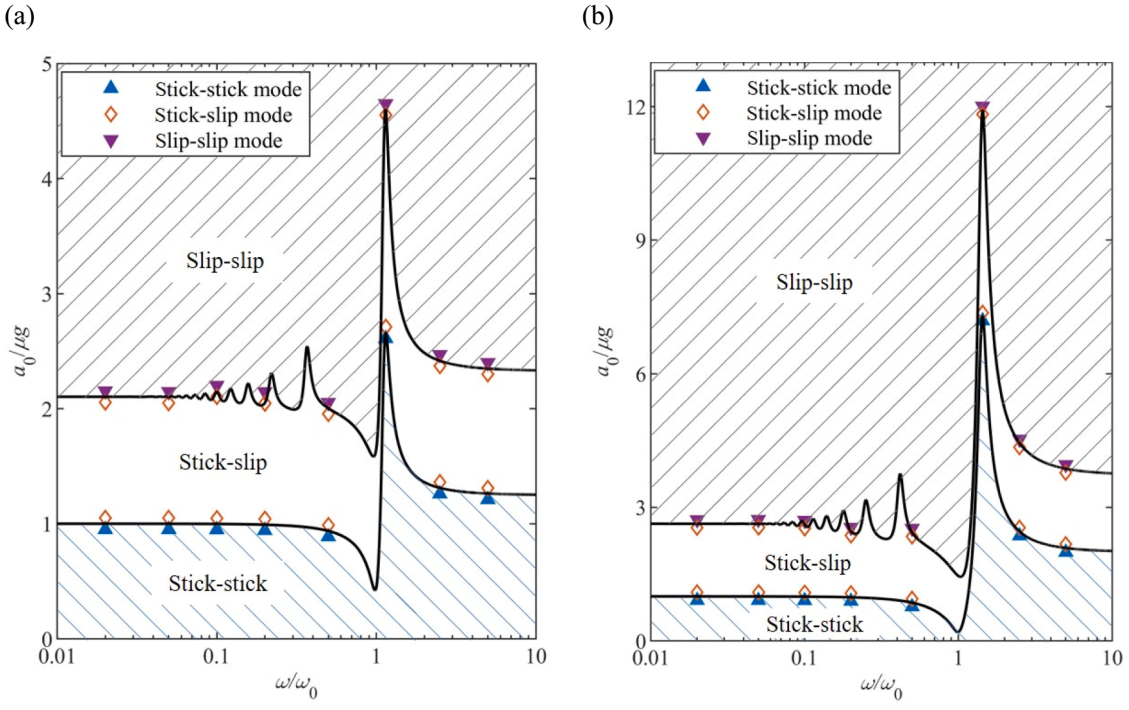

Fig. 7. Regions for three modes of inerter-added sliding isolation structures, computed for the damping ratio of the superstructure of $\zeta_0 = 0.05$, where both the numerical simulation and analytical solutions expressed by Eqs. (43)–(45) are used: (a) structural parameters with $\alpha = 0.2$ and $\beta = 0.2$, and (b) structural parameters with $\alpha = 0.5$ and $\beta = 0.4$.

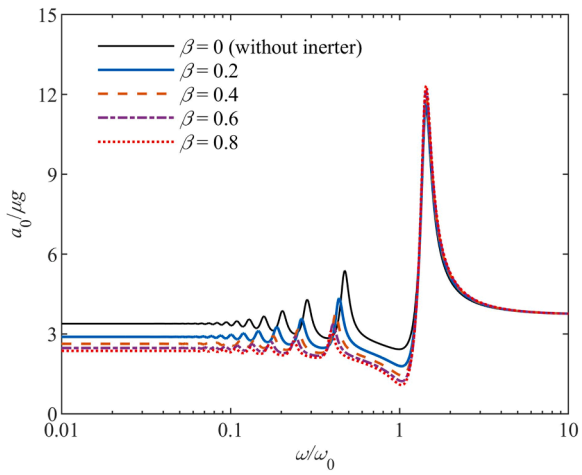

Fig. 8. Boundaries between the stick-slip and slip-slip motion modes of the inerter-added sliding isolation structures for different values of β with the structural parameters of $\alpha = 0.5$ and $\zeta_0 = 0.05$, where the analytical solution for determining structural motion modes in Eq. (42) is adopted.

than those in Fig. 7(a). This means that the slip-stick and slip-slip modes occur harder for a larger value of α. A large value of α usually indicates that the weight of the sliding base is large. Hence, a large value of the friction force is required to start the slippage of the sliding system. The slippage-related motion modes of the sliding system occur harder for a larger value of α. Since this study is focused on the object of an additional inerter, detailed parametric analyses involving the mass ratio α are not presented. Scholars interested in this point can see the investigations in the literature [61,63]. In addition, since the boundaries between the stick-stick and stick-slip modes indicated by both the analytical and numerical results match well in Fig. 7, this also validates that adding an inerter will not alter the occurrence conditions of the stick-stick mode of sliding isolation structures.

4. Influence of additional inerter in sliding isolation structures

Based on the derivations above, the dynamic characteristics of structures are adjusted during slippage phases, and the structural motion modes are affected by adding an inerter in sliding isolation structures. To provide a qualitative study, in this section, the influences of the additional inerter on the motion modes and the significant responses of the sliding isolation structure are investigated through extensive parametric analyses based on the derived closed-form solutions. Some design recommendations are also provided.

4.1. Influence of the inerter on the conditions for motion modes

It is indicated that the additional inerter will not affect the boundary between the stick-stick and stick-slip modes of the sliding isolation structure according to the analyses above. Hence, the influences of the additional inerter on the boundaries between the stick-slip and slip-slip modes are only analyzed here. For inerter-added sliding isolation structures with parameters of $\alpha = 0.5$ and $\zeta_0 = 0.05$, the boundaries between the stick-slip and slip-slip modes are shown in Fig. 8 by depicting relationships between the frequency ratio ω/ω_0 and normalized excitation amplitude $a_0/\mu g$ for different inertance-to-mass ratios β. The shapes of the boundaries between the stick-slip and slip-slip modes are similar for different values of β. These boundaries exhibit multiple peaks when ω/ω_0 is less than 1, and the maximum peak values of $a_0/\mu g$ occur for values of ω/ω_0 between 1 and 2. The boundaries for sliding isolation structures without an inerter (i.e., $\beta = 0$) have the largest $a_0/\mu g$ for most values of ω/ω_0 less than 1. In addition, for these regions of ω/ω_0 less than 1, boundaries represented by $a_0/\mu g$ decrease with the increase of β for fixed ω/ω_0. This indicates that the slip-slip mode of the inerter-added sliding isolation structure can occur with a lower excitation amplitude by increasing the inertance of the inerter for most values of ω/ω_0 less than 1. With the increase in the amplitude of the harmonic ground excitation under a specific frequency for a sliding isolation system, the rate of increase of the relative sliding displacement during the slip-slip mode is smaller than that during the stick-slip mode. The relevant analyses are shown in the subsequent section in detail. Similar results can also be found in previous work [61]. In this regard, the slip-slip mode is preferred compared to the stick-slip mode for a sliding isolation system [7,61]. Consequently, adding an inerter is beneficial for sliding isolation structures in most situations of ω/ω_0 less than 1. When the values of ω/ω_0 are far larger than 1, the boundaries for different values of β are almost coincident. This means that the additional inerter has little influence on the occurrence conditions of the slip-slip mode for sliding isolation structures when the values of ω/ω_0 are far larger than 1. For $\omega/\omega_0 \gg 1$, the frequency of the superstructure is quite small, i.e., the superstructure is very flexible. For such a structure with a sliding base, the acceleration of this system is small and not sensitive to the ground motion excitation. Since the output force of the inerter is acceleration dependent, the influence of the additional inerter on the response of such a sliding system is weak. However, considering that seismic isolation technology is usually not recommended for long-period structures, application scenarios of inerters in such structures are rare.

4.2. Influence of the inerter on the responses of sliding isolation structures

Adding an inerter can adjust the structural dynamic characteristics of sliding isolation structures during slippage phases. As a result, the structural responses are impacted by the additional inerter. The absolute acceleration of the primary mass $\ddot{x}$ (related to the structural base shear force) and the displacement of the isolation layer y_b are two aspects of the performance of isolation structures in this study. For convenience of analyses, the performance indices involving these two responses are defined with dimensionless forms. For the index of $\ddot{x}$, the normalized maximum acceleration $A_p/\mu g$ is adopted for evaluation, which is calculated as

$$\frac{A_p}{\mu g} = \frac{\max|\ddot{x}|}{\mu g} \tag{48}$$

where A_p is the maximum value of the absolute acceleration $\ddot{x}$. For the index of y_b, the normalized isolation displacement amplitude $y_{b,ap}/(a_0/\omega_0^2)$ is employed to evaluate the structural performance, where a_0/ω_0^2 denotes the amplitude of the ground motion displacement. Analyses conducted here are focused on the influences of additional inerters and the characteristics of harmonic ground motions on the responses of inerter-added sliding isolation structures. All the analyses below are performed using the solutions in the structure steady state.

4.2.1. Maximum pseudoacceleration of superstructure

According to the solutions of the inerter-added sliding isolation structures given in Section 2.2, the structural responses are related to the values of α, μg, ζ_0, β, ω/ω_0 and a_0. Fig. 9(a) shows the relationships between the normalized maximum acceleration $A_p/\mu g$ and frequency ratio ω/ω_0 for different values of β with $\alpha = 0.5$, $\zeta_0 = 0.05$ and $a_0/\mu g = 2$. Several resonant frequency ratios exist for inerter-added sliding isolation structures when sliding occurs, which is quite different from fixed base structures. In Fig. 9(a), the resonant frequency ratios shift toward lower values of ω/ω_0 as β increases. This is because the frequency $\omega_1 = \omega_0\sqrt{(1+\beta)/(1+\beta-\alpha)}$ during the slippage phase decreases with increasing β. For the largest several (especially the largest two) resonant frequency ratios, the corresponding peak values of $A_p/\mu g$ for the inerter-added sliding isolation structure are larger than those of the sliding isolation structure without an inerter (i.e., $\beta = 0$). Except for

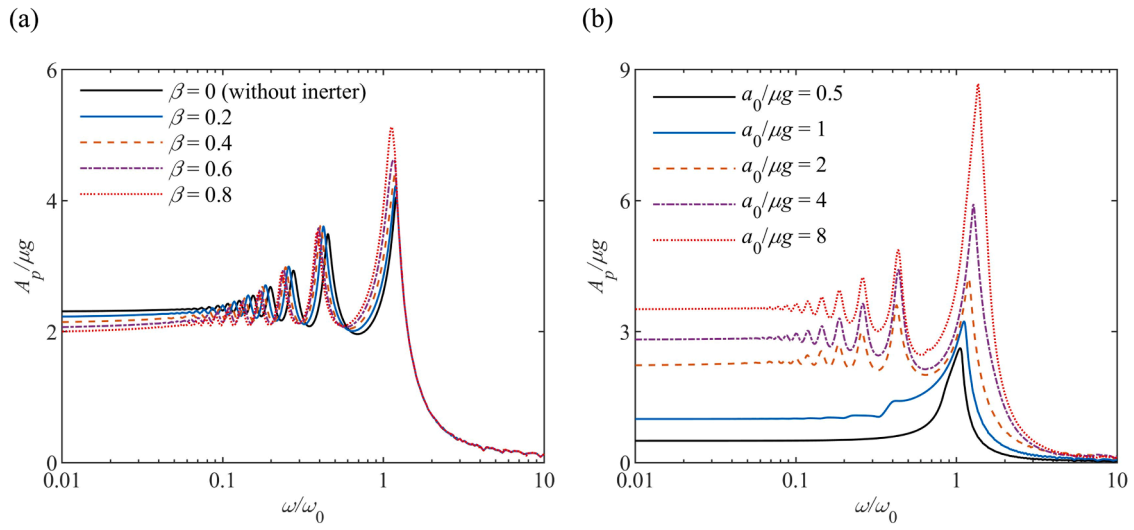

Fig. 9. Relationships between normalized maximum acceleration $A_p/\mu g$ and frequency ratio ω/ω_0 for inerter-added sliding isolation structures, where the derived closed-form solutions for structural responses are used: (a) Different values of β for $\alpha = 0.5$, $\zeta_0 = 0.05$ and $a_0/\mu g = 2$, and (b) different values of $a_0/\mu g$ for $\alpha = 0.5$, $\zeta_0 = 0.05$ and $\beta = 0.2$.

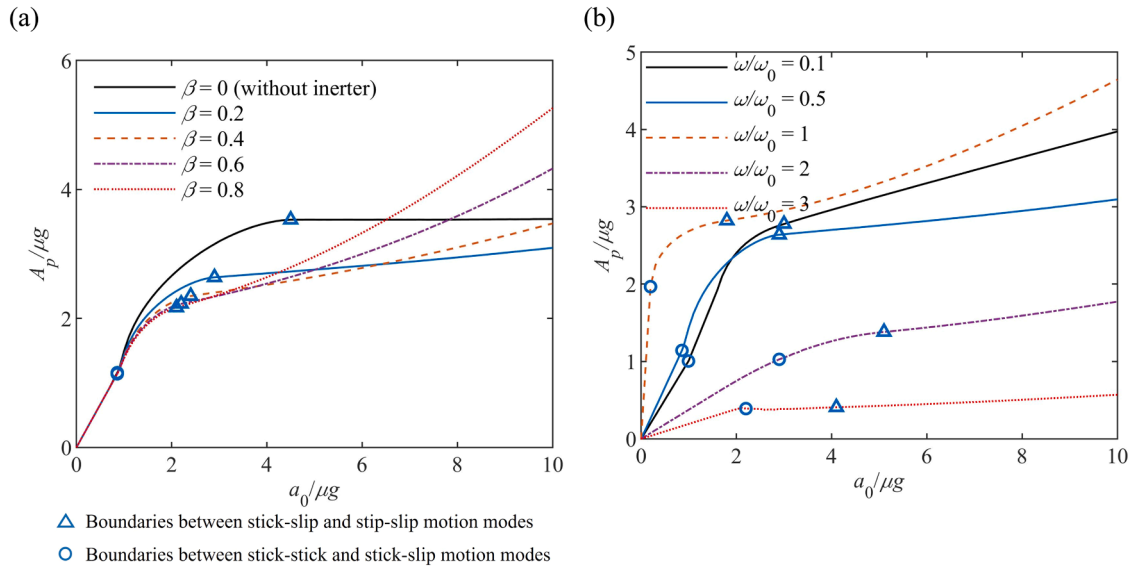

Fig. 10. Relationships between the normalized maximum acceleration $A_p/\mu g$ and normalized excitation amplitude $a_0/\mu g$ for inerter-added sliding isolation structures, where the derived closed-form solutions for structural responses are used: (a) Different values of β for $\alpha = 0.5$, $\zeta_0 = 0.05$ and $\omega/\omega_0 = 0.5$; (b) different values of ω/ω_0 for $\alpha = 0.5$, $\zeta_0 = 0.05$ and $\beta = 0.2$.

the largest resonant frequency ratio, the peak values of $A_p/\mu g$ in the corresponding resonant frequency ratios decrease with increasing β for inerter-added sliding isolation structures. Additionally, in the region of small frequency ratio ω/ω_0 ($\omega/\omega_0 \leq 1$), the values of $A_p/\mu g$ for inerter-added sliding isolation structures are lower than those of the sliding isolation structure without an inerter (i.e., $\beta = 0$), and $A_p/\mu g$ decreases with the increase of β for a certain ω/ω_0. In the region of large ω/ω_0, the values of $A_p/\mu g$ are almost the same for different values of β for a specific ω/ω_0. This phenomenon can be attributed to the flexible superstructure for $\omega/\omega_0 \gg 1$. The acceleration of a flexible structure isolated with the sliding base is usually small and not sensitive to the ground motion excitation. Considering that the mechanical behavior of the inerter is acceleration dependent, the influence of the additional inerter on the response of such a sliding system is weak. In some regions of $0.1 \leq \omega/\omega_0 \leq 1$, the performance of inerter-added sliding isolation structures regarding $A_p/\mu g$ are superior to those of the sliding isolation structure without an inerter (i.e., $\beta = 0$) but worse in the other regions of $0.1 \leq \omega/\omega_0 \leq 1$. Hence, with the goal of reducing the responses of $A_p/\mu g$, it is recommended to move the frequency ratio ω/ω_0 away from these regions of worse performance and resonant frequency ratios (especially the largest two).

The relationships between $A_p/\mu g$ and ω/ω_0 for different values of $a_0/\mu g$ are shown in Fig. 9(b) by setting $\alpha = 0.5$, $\zeta_0 = 0.05$ and $\beta = 0.2$. The curves for large $a_0/\mu g$ also have several resonant frequency ratios in which sliding occurs. The values of resonant frequency ratios are almost the same for values of $a_0/\mu g$ equal to 2, 4 and 8 because the values of α and β that are related to the structural frequencies are unchanged. Since the stick-stick mode appears mainly for $a_0/\mu g$ equal to 0.5 and 1, there are single resonant frequency ratios for these two curves. In addition, the value of $A_p/\mu g$ for a specific ω/ω_0 increases with increasing $a_0/\mu g$ for the inerter-added sliding isolation structure.

Fig. 10(a) and Fig. 10(b) show the relationships between $A_p/\mu g$ and

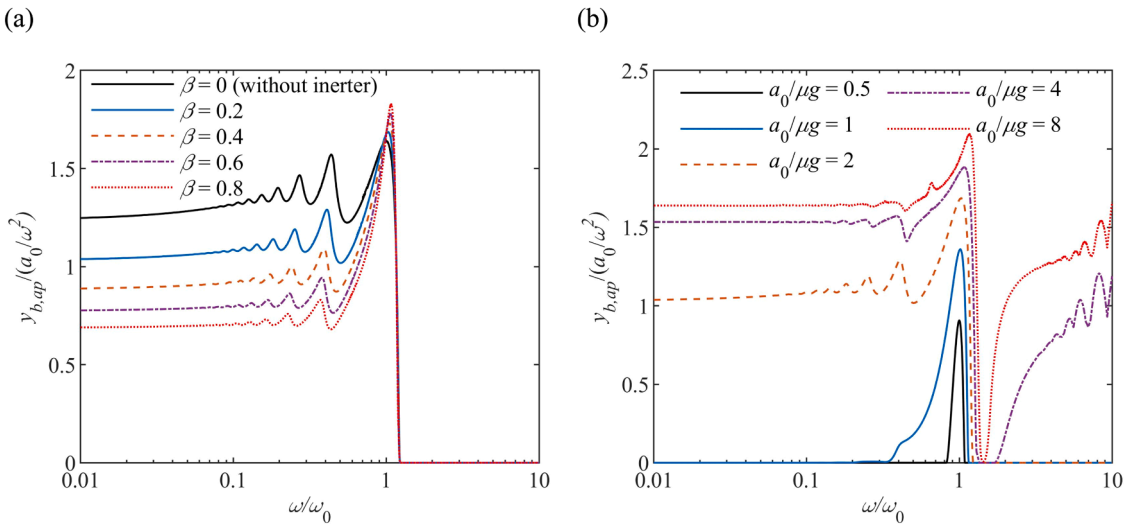

Fig. 11. Relationships between the normalized isolation displacement amplitude $y_{b,ap}/(a_0/\omega^2)$ and normalized excitation amplitude ω/ω_0 for inerter-added sliding isolation structures, where the derived closed-form solutions for structural responses are used: (a) Different values of β for α = 0.5, ζ_0 = 0.05 and $a_0/\mu g$ = 2; (b) different values of $a_0/\mu g$ for α = 0.5, ζ_0 = 0.05 and β = 0.2.

$a_0/\mu g$ for different values of β and ω/ω_0, respectively. The boundaries between stick-stick and stick-slip modes and boundaries between stick-slip and slip-slip modes are marked in the relationship curves using circle and triangle symbols, respectively. Consequently, these curves in Fig. 10 are separated into three regions that are related to motions with stick-stick, stick-slip and slip-slip modes. In Fig. 10(a), the $A_p/\mu g$ versus $a_0/\mu g$ curves for different values of β with stick-stick mode are straight lines and overlap. The boundaries for the stick-stick and stick-slip modes are also the same for different β. This supports the previous conclusions that adding an inerter in sliding isolation structures will not affect the responses of structures in stick phases and boundaries between stick-stick and stick-slip modes. For the sliding isolation structure without an inerter (β = 0), the value of $A_p/\mu g$ is constant in the region of the slip-slip mode, whereas for inerter-added sliding isolation structures, the values of $A_p/\mu g$ for a specific βincrease with increasing $a_0/\mu g$. Additionally, the corresponding increase rates of these curves with slip-slip mode increase with the increase in $A_p/\mu g$, as well as the value of β. Hence, a larger β is not always beneficial for reducing the response with respect to $A_p/\mu g$, especially under ground motions with large amplitudes. In Fig. 10(b), the value of $A_p/\mu g$ for the curve of $\omega/\omega_0 = 1$ is larger than the other curves for a certain $a_0/\mu g$. For the curves of $\omega/\omega_0 = 2$ and $\omega/\omega_0 = 3$, the values of $A_p/\mu g$ are smaller than the other curves for a certain $a_0/\mu g$. This is due to the resonant phenomena that exist for $\omega/\omega_0 < 1$ and the largest peak for the resonant frequency ratio near $\omega/\omega_0 = 1$.

4.2.2. *Amplitude of the relative displacement of the sliding base*

Fig. 11(a) shows the relationships between the normalized isolation displacement amplitude $y_{b,ap}/(a_0/\omega^2)$ and frequency ratio ω/ω_0 for different values of β with α = 0.5, ζ_0 = 0.05 and $a_0/\mu g$ = 2. It can be seen that the values of $y_{b,ap}/(a_0/\omega^2)$ for the sliding isolation structure without an inerter (i.e., β = 0) are larger than those for the inerter-added sliding isolation structures. The values of $y_{b,ap}/(a_0/\omega^2)$ decrease with the increase in β for a certain ω/ω_0 in most regions of $\omega/\omega_0 < 1$. In a

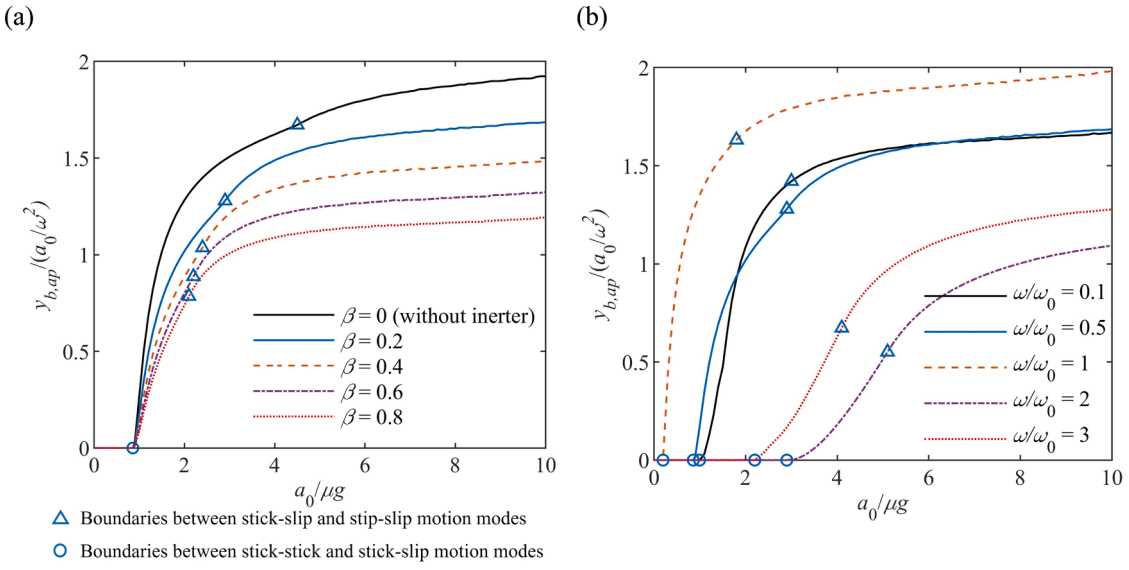

Fig. 12. Relationships between the normalized isolation displacement amplitude $y_{b,ap}/(a_0/\omega^2)$ and normalized excitation amplitude $a_0/\mu g$ for inerter-added sliding isolation structures, where the derived closed-form solutions for structural responses are used: (a) Different values of β for α = 0.5, ζ_0 = 0.05 and ω/ω_0 = 0.5; (b) different values of ω/ω_0 for α = 0.5, ζ_0 = 0.05 and β = 0.2.

small region of ω/ω_0 near 1, the values of $y_{b,ap}/(a_0/\omega^2)$ increase as the value of β increases. In general, the additional inerter can effectively reduce the displacement of the isolation layer. The zero value of $y_{b,ap}/(a_0/\omega^2)$ indicates the stick-stick motion mode of the inerter-added sliding isolation structure, which occurs in the same region of large values of ω/ω_0 for curves with different β in Fig. 11(a). This is because the additional inerter does not affect the occurrence condition of the stick-stick mode. Fig. 11(b) shows the relationships between $y_{b,ap}/(a_0/\omega^2)$ and ω/ω_0 for different values of $a_0/\mu g$ with $\alpha = 0.5$, $\zeta_0 = 0.05$ and $\beta = 0.2$. Sliding occurs more easily for values of ω/ω_0 close to 1 (seen curves of $a_0/\mu g = 0.5$ and $a_0/\mu g = 1$ in Fig. 11(b)). The influence of the values of ω/ω_0 on the normalized isolation displacement amplitude $y_{b,ap}/(a_0/\omega^2)$ is not significant for a large $a_0/\mu g$ when $\omega/\omega_0 < 1$. After the value of ω/ω_0 exceeds 1, the value of $y_{b,ap}/(a_0/\omega^2)$ decreases notably as ω/ω_0 increases. This is consistent with the results in Fig. 8, where the occurrence condition of the stick-slip mode indicated by $a_0/\mu g$ increases with the increase in ω/ω_0 after ω/ω_0 exceeds 1. When ω/ω_0 continuously increases beyond a critical value, the value of $y_{b,ap}/(a_0/\omega^2)$ tends to increase as ω/ω_0 increases for large $a_0/\mu g$. This is also consistent with the curve in Fig. 8, where the condition of the slip-slip mode expressed by $a_0/\mu g$ decreases as ω/ω_0 increases in the region of large ω/ω_0.

The relationships between $y_{b,ap}/(a_0/\omega^2)$ and $a_0/\mu g$ for different values of β with $\alpha = 0.5$, $\zeta_0 = 0.05$ and $a_0/\mu g = 2$ are shown in Fig. 12(a). For a larger β, the value of $y_{b,ap}/(a_0/\omega^2)$ is smaller for a fixed $a_0/\mu g$ in both regions of the stick-slip and slip-slip modes. The additional inerter can be beneficial for reducing the isolation displacement when sliding occurs. Fig. 12(a) shows the relationships between $y_{b,ap}/(a_0/\omega^2)$ and $a_0/\mu g$ for different values of ω/ω_0 with $\alpha = 0.5$, $\zeta_0 = 0.05$ and $a_0/\mu g = 2$. It is seen that the value of $y_{b,ap}/(a_0/\omega^2)$ for the curve of $\omega/\omega_0 = 1$ is the largest for the presented curves with different values of ω/ω_0. For the curves of $\omega/\omega_0 = 2$ and $\omega/\omega_0 = 3$, the values of $y_{b,ap}/(a_0/\omega^2)$ are smaller than the other curves for a certain $a_0/\mu g$. These tendencies of the normalized isolation displacement amplitude $y_{b,ap}/(a_0/\omega^2)$ for different ω/ω_0 are similar to those of the normalized maximum acceleration $A_p/\mu g$. In addition, the value of $y_{b,ap}/(a_0/\omega^2)$ increases with increasing $a_0/\mu g$ for all the curves in Fig. 12. The corresponding increase rate of the curve in the slip-slip mode is clearly smaller than that in the stick-slip mode. From this perspective, the slip-slip mode will be preferred compared to the stick-slip mode considering the increasing tendency of isolation displacement. Hence, an easier occurrence condition of the slip-slip mode induced by adding an inerter can be beneficial for reducing the isolation displacement. However, an additional inerter with a large β is not desired for mitigating the normalized maximum acceleration considering the rapid increase in $A_p/\mu g$ in the slip-slip mode, as shown in Fig. 10(a). Hence, an appropriate value of β for the additional inerter rather than a large β is recommended for application considering the trade-off of performances between the isolation displacement and acceleration.

Using the sliding isolation structure with $\alpha = 0.5$ and $\zeta_0 = 0.05$ as an example, we give a detailed illustration for selecting the value of inertance of the additional inerter in the design scenario herein. In Figs. 11(a) and 12(a), the isolation displacements decrease with increasing β for a certain ω/ω_0 in most regions of $\omega/\omega_0 < 1$. In addition, a clear reduction of the isolation displacements is shown for $\beta \geq 0.2$. Hence, considering the reduction of the isolation displacement, the value of the inertance to mass ratio β should be selected as large as possible and larger than 0.2. However, for the acceleration response of the sliding isolation structure, the rates of increase for the curves during slip-slip mode regions in Fig. 10(a) increase with the increase in the value of β. When the value of β is larger than 0.4, the acceleration response of the inerter-added sliding isolation structure is larger than that of the sliding isolation structure without inerter ($\beta = 0$), as shown in Fig. 10(a). Hence, to not amplify the acceleration response, a value of β less than 0.4 is recommended. As a result, the recommendation for the range of the value of β is from 0.2 to 0.4 considering the tradeoff between the reduction of isolation displacement and acceleration. For a better reduction of the isolation displacement, the value of β is recommended close to 0.4, whereas for a better reduction of the acceleration, the value of β is recommended close to 0.2. Note that the design consideration above is illustrated based on the parametric analyses within the range of the frequency ratio of $\omega/\omega_0 < 1$.

5. Conclusions

This study has addressed the analytical solutions of inerter-added sliding isolation structures subjected to harmonic ground motions, which assists the understanding of the inherent mechanism of the additional inerter in a sliding isolation structure. For the inerter-added sliding isolation structure, the inerter installed between the base floor and the ground is adopted to improve the structural performance compared to the traditional sliding isolation structure. The mechanical model of the inerter-added sliding isolation structure is built, and the corresponding governing equations of motion are derived for both the stick and slippage phases of the structure. The dynamic characteristic parameters of the inerter-added sliding isolation structure indicate the likely superiority of structural performance over traditional sliding isolation structures. Closed-form solutions for dynamic responses are obtained by solving the governing equations of motion. Subsequently, the three motion modes of the inerter-added sliding isolation structure (i.e., the stick-stick, stick-slip and slip-slip modes) are described. By employing the steady-state responses of the structure, explicit expressions for the occurrence conditions of these three modes are derived. Parametric analyses are conducted to analyze the influence of the inerter on the occurrence conditions of structural motion modes. To assess the performance of the inerter-added sliding isolation structure, structural responses, including superstructure acceleration and displacement of the sliding base, are analyzed for different values of inertance and different loading parameters, in which the response indicators are of significant interest in design scenarios for engineers.

Throughout the paper, the investigations are conducted based on the derived closed-form solutions of the inerter-added sliding isolation structure, which is considered useful for exploring the working mechanism of the additional inerter but not carried out previously for such structures. Adding an inerter to the sliding isolation structure can reduce the ground motion excitation transferred to the superstructure. By increasing the inertance of the additional inerter, the slip-slip mode of the inerter-added sliding isolation structure will occur at a lower amplitude of the harmonic ground motion. This reveals the role of the additional inerter played in a sliding isolation system that makes the slip-slip mode occur more easily. The analysis results indicate that the inerter-added sliding isolation structure exhibits several resonant frequencies when sliding occurs. The increase in the inertance of the inerter leads to a decrease in the isolation displacement in both the stick-stick and slip-slip modes of the inerter-added sliding isolation structure. However, a large inertance of the inerter causes a rapid increase in the maximum acceleration as the amplitude of the ground motion increases in the slip-slip mode. As a result, the structural frequency should be moved away from the observed resonant frequencies for designing an inerter-added sliding isolation structure. Considering the trade-off of the isolation displacement and maximum acceleration for determining the inertance of the additional inerter is recommended.

The conclusions of the inerter-added sliding isolation structures obtained in this study are limited to the harmonic ground motion excitations. When the structures are subjected to earthquake excitations, the responses of inerter-added sliding isolation structures can be different from those obtained under harmonic ground motions. The analytical solutions derived in this study are not applicable for earthquake excitations. However, the exploration of the analytical solutions for the inerter-added sliding isolation structure under harmonic ground

motions can provide insight into how this structure will respond to earthquake excitations. Furthermore, the theoretical results of the inerter-added sliding isolation structure obtained under harmonic ground motions can be used to make design decisions for the structure under earthquake excitations. Research involving the analytical solutions of inerter-added sliding isolation structures under seismic excitations deserves further investigation in the near future.

CRediT authorship contribution statement

Songtao Xue: Conceptualization, Methodology, Investigation, Writing – review & editing, Funding acquisition. **Li Zhang:** Conceptualization, Methodology, Investigation, Software, Writing – original draft, Writing – review & editing, Formal analysis, Visualization. **Liyu Xie:** Methodology, Writing – review & editing, Funding acquisition, Validation. **Ruifu Zhang:** Conceptualization, Methodology, Writing – review & editing, Funding acquisition, Visualization. **Jianfei Kang:** Software, Investigation, Writing – review & editing, Validation.

Declaration of Competing Interest

The authors declare no conflict of interest.

Data availability

Data will be made available on request.

Acknowledgments

This study was supported by the National Natural Science Foundation of China (Grant No. 51978525), the National Key R&D Program of China (Grant No. 2021YFE0112200) and the Scientific Research Fund of Institute of Engineering Mechanics, China Earthquake Administration (Grant No. 2020EEEVL0401, 2019EEVL03 and 2019D14).

References

[1] Kelly JM. Aseismic base isolation: review and bibliography. Soil Dyn Earthq Eng 1986;5:202–16. https://doi.org/10.1016/0267-7261(86)90006-0.
[2] Makris N, Chang SP. Effect of viscous, viscoplastic and friction damping on the response of seismic isolated structures. Earthq Eng Struct Dyn 2000;29:85–107. https://doi.org/10.1002/(SICI)1096-9845(200001)29:1.85::AID-EQE902.3.0.CO;2-N.
[3] Zhang R, Wu M, Lu W, Li X, Lu X. Seismic retrofitting of a historic building by using an isolation system with a weak restoring force. Soil Dyn Earthq Eng 2021;148:106836. https://doi.org/10.1016/j.soildyn.2021.106836.
[4] De Luca A, Guidi LG. State of art in the worldwide evolution of base isolation design. Soil Dyn Earthq Eng 2019;125:105722. https://doi.org/10.1016/j.soildyn.2019.105722.
[5] Mostaghel N, Hejazi M, Tanbakuchi J. Response of sliding structures to harmonic support motion. Earthq Eng Struct Dyn 1983;11:355–66. https://doi.org/10.1002/eqe.4290110305.
[6] Constantinou M, Mokha A, Reinhorn A. Teflon bearings in base isolation II: modeling. J Struct Eng 1990;116:455–74. https://doi.org/10.1061/(ASCE)0733-9445(1990)116:2(455).
[7] Zhang C, Ali A. The advancement of seismic isolation and energy dissipation mechanisms based on friction. Soil Dyn Earthq Eng 2021;146:106746. https://doi.org/10.1016/j.soildyn.2021.106746.
[8] Iemura H, Taghikhany T, Jain SK. Optimum design of resilient sliding isolation system for seismic protection of equipments. Bull Earthq Eng 2007;5:85–103. https://doi.org/10.1007/s10518-006-9010-5.
[9] Mostaghel N, Khodaverdian M. Dynamics of resilient-friction base isolator (R-FBI). Earthq Eng Struct Dyn 1987;15:379–90. https://doi.org/10.1002/eqe.4290150307.
[10] Makris N. Seismic isolation: early history. Earthq Eng Struct Dyn 2019;48:269–83. https://doi.org/10.1002/eqe.3124.
[11] Dolce M, Cardone D, Palermo G. Seismic isolation of bridges using isolation systems based on flat sliding bearings. Bull Earthq Eng 2007;5:491–509. https://doi.org/10.1007/s10518-007-9044-3.
[12] Li L. Base isolation measure for aseismic buildings in China. In: Proceedings of 8th world conference on earthquake engineering. San Francisco, California, 1984.
[13] Banović I, Radnić J, Grgić N, Matešan D. The use of limestone sand for the seismic base isolation of structures. Adv Civ Eng 2018:9734283. https://doi.org/10.1155/2018/9734283. 2018.
[14] Kuvat A, Sadoglu E. Dynamic properties of sand-bitumen mixtures as a geotechnical seismic isolation material. Soil Dyn Earthq Eng 2020;132:106043. https://doi.org/10.1016/j.soildyn.2020.106043.
[15] Tsang HH, Tran DP, Hung WY, Pitilakis K, Gad EF. Performance of geotechnical seismic isolation system using rubber-soil mixtures in centrifuge testing. Earthq Eng Struct Dyn 2021;50:1271–89. https://doi.org/10.1002/eqe.3398.
[16] Tsang HH. Seismic isolation by rubber–soil mixtures for developing countries. Earthq Eng Struct Dyn 2008;37:283–303. https://doi.org/10.1002/eqe.756.
[17] Xiong W, Li Y. Seismic isolation using granulated tire–soil mixtures for less-developed regions: experimental validation. Earthq Eng Struct Dyn 2013;42:2187–93. https://doi.org/10.1002/eqe.2315.
[18] Tsiavos A, Sextos A, Stavridis A, Dietz M, Dihoru L, Di Michele F, et al. Low-cost hybrid design of masonry structures for developing countries: shaking table tests. Soil Dyn Earthq Eng 2021;146:106675. https://doi.org/10.1016/j.soildyn.2021.106675.
[19] Anagnostopoulos SA, Spiliopoulos KV. An investigation of earthquake induced pounding between adjacent buildings. Earthq Eng Struct Dyn 1992;21:289–302. https://doi.org/10.1002/eqe.4290210402.
[20] Kelly JM. The role of damping in seismic isolation. Earthq Eng Struct Dyn 1999;28:3–20. https://doi.org/10.1002/(SICI)1096-9845(199901)28:1.3::AID-EQE801.3.0.CO;2-D.
[21] Taniguchi T, Der Kiureghian A, Melkumyan M. Effect of tuned mass damper on displacement demand of base-isolated structures. Eng Struct 2008;30:3478–88. https://doi.org/10.1016/j.engstruct.2008.05.027.
[22] Xiang P, Nishitani A. Optimum design for more effective tuned mass damper system and its application to base-isolated buildings. Struct Control Health Monit 2014;21:98–114. https://doi.org/10.1002/stc.1556.
[23] Zhao Z, Zhang R, Wierschem NE, Jiang Y, Pan C. Displacement mitigation-oriented design and mechanism for inerter-based isolation system. J Vib Control 2021;27:1991–2003. https://doi.org/10.1177/1077546320951662.
[24] Zhao Z, Chen Q, Zhang R, Pan C, Jiang Y. Optimal design of an inerter isolation system considering the soil condition. Eng Struct 2019;196:109324. https://doi.org/10.1016/j.engstruct.2019.109324.
[25] De Domenico D, Ricciardi G. An enhanced base isolation system equipped with optimal tuned mass damper inerter (TMDI). Earthq Eng Struct Dyn 2018;47:1169–92. https://doi.org/10.1002/eqe.3011.
[26] Ikago K, Saito K, Inoue N. Seismic control of single-degree-of-freedom structure using tuned viscous mass damper. Earthq Eng Struct Dyn 2012;41:453–74. https://doi.org/10.1002/eqe.1138.
[27] Pan C, Zhang RF, Luo H, Li C, Shen H. Demand-based optimal design of oscillator with parallel-layout viscous inerter damper. Struct Control Health Monit 2018;25:e2051. https://doi.org/10.1002/Stc.2051.
[28] Pan C, Zhang R. Design of structure with inerter system based on stochastic response mitigation ratio. Struct Control Health Monit 2018;25:e2169. https://doi.org/10.1002/stc.2169.
[29] Saito K., Sugimura Y., Nakaminami S., Kida H., Inoue N. Vibration tests of 1-story response control system using inertial mass and optimized soft spring and viscous element. In: Proceedings of the 14th world conference on earthquake engineering. Beijing, China, 2008.
[30] Zhao Z, Chen Q, Zhang R, Jiang Y, Pan C. A negative stiffness inerter system (NSIS) for earthquake protection purposes. Smart Struct Syst 2020;26:481–93. https://doi.org/10.12989/sss.2020.26.4.481.
[31] Zhang L, Xue S, Zhang R, Hao L, Pan C, Xie L. A novel crank inerter with simple realization: constitutive model, experimental investigation and effectiveness assessment. Eng Struct 2022;262:114308. https://doi.org/10.1016/j.engstruct.2022.114308.
[32] Zhang R, Zhang L, Pan C, De Domenico D, Chen Q. Targeted modal response control of structures using inerter systems based on master oscillator principle. Int J Mech Sci 2021;206:106636. https://doi.org/10.1016/j.ijmecsci.2021.106636.
[33] Zhao Z, Zhang R, Lu Z. A particle inerter system for structural seismic response mitigation. J Franklin Inst 2019;356:7669–88. https://doi.org/10.1016/j.jfranklin.2019.02.001.
[34] De Domenico D, Deastra P, Ricciardi G, Sims ND, Wagg DJ. Novel fluid inerter based tuned mass dampers for optimised structural control of base-isolated buildings. J Franklin Inst 2019;356:7626–49. https://doi.org/10.1016/j.jfranklin.2018.11.012.
[35] Zhang RF, Zhao ZP, Pan C, Ikago K, Xue ST. Damping enhancement principle of inerter system. Struct Control Health Monit 2020;27:e2523. https://doi.org/10.1002/stc.2523.
[36] Cao L, Li C. Tuned tandem mass dampers-inerters with broadband high effectiveness for structures under white noise base excitations. Struct Control Health Monit 2019;26(4):e2319. https://doi.org/10.1002/stc.2319.
[37] Zhao ZP, Zhang RF, Jiang YY, Pan C. A tuned liquid inerter system for vibration control. Int J Mech Sci 2019;164:105171. https://doi.org/10.1016/j.ijmecsci.2019.105171.
[38] Wang Q, Tiwari ND, Qiao H, Wang Q. Inerter-based tuned liquid column damper for seismic vibration control of a single-degree-of-freedom structure. Int J Mech Sci 2020;184:105840. https://doi.org/10.1016/j.ijmecsci.2020.105840.
[39] Wang H, Gao H, Li J, Wang Z, Ni Y, Liang R. Optimum design and performance evaluation of the tuned inerter-negative-stiffness damper for seismic protection of single-degree-of-freedom structures. Int J Mech Sci 2021;212:106805. https://doi.org/10.1016/j.ijmecsci.2021.106805.

[40] Hu Y, Chen MZQ. Performance evaluation for inerter-based dynamic vibration absorbers. Int J Mech Sci 2015;99:297–307. https://doi.org/10.1016/j.ijmecsci.2015.06.003.
[41] Takino M, Asai T. Development and performance evaluation of an electromagnetic transducer with a tuned variable inerter. J Vib Control 2022. https://doi.org/10.1177/10775463221074078. 10775463221074078.
[42] Javidialesaadi A, Wierschem NE. An inerter-enhanced nonlinear energy sink. Mech Syst Signal Process 2019;129:449–54. https://doi.org/10.1016/j.ymssp.2019.04.047.
[43] Lazarek M, Brzeski P, Perlikowski P. Design and identification of parameters of tuned mass damper with inerter which enables changes of inertance. Mech Mach Theory 2018;119:161–73. https://doi.org/10.1016/j.mechmachtheory.2017.09.004.
[44] Zhang R, Zhao Z, Dai K. Seismic response mitigation of a wind turbine tower using a tuned parallel inerter mass system. Eng Struct 2019;180:29–39. https://doi.org/10.1016/j.mechmachtheory.2017.09.004.
[45] Zhang L, Xue S, Zhang R, Xie L, Hao L. Simplified multimode control of seismic response of high-rise chimneys using distributed tuned mass inerter systems (TMIS). Eng Struct 2021;228:111550. https://doi.org/10.1016/j.engstruct.2020.111550.
[46] He H, Li Y, Jiang JZ, Burrow S, Neild S, Conn A. Using an inerter to enhance an active-passive-combined vehicle suspension system. Int J Mech Sci 2021;204:106535. https://doi.org/10.1016/j.ijmecsci.2021.106535.
[47] Ning D, Sun S, Du H, Li W, Zhang N, Zheng M, et al. An electromagnetic variable inertance device for seat suspension vibration control. Mech Syst Signal Process 2019;133:106259. https://doi.org/10.1016/j.ymssp.2019.106259.
[48] Zhang R, Zhao Z, Lin X, Zhang L. Optimal design of inerter systems for the force-transmission suppression of oscillating structures. Earthq Eng Eng Vib 2022;21:441–54. https://doi.org/10.1007/s11803-022-2090-7.
[49] Zhang R, Ke Y, Li Z, Guo M. Vibration mitigation of waterflood pump station based on inerter system. In: Energy China forum 2021 11th Asia-Pacific shale & unconventional resources summit. Shanghai, China; 2021.
[50] Cao L, Li C. A high performance hybrid passive base-isolated system. Struct Control Health Monit 2022;29:e2887. https://doi.org/10.1002/stc.2887.
[51] Li C, Chang K, Cao L, Huang Y. Performance of a nonlinear hybrid base isolation system under the ground motions. Soil Dyn Earthq Eng 2021;143:106589. https://doi.org/10.1016/j.soildyn.2021.106589.
[52] Saitoh M. On the performance of gyro-mass devices for displacement mitigation in base isolation systems. Struct Control Health Monit 2012;19:246–59. https://doi.org/10.1002/stc.419.
[53] Ye K, Shu S, Hu L, Zhu H. Analytical solution of seismic response of base-isolated structure with supplemental inerter. Earthq Eng Struct Dyn 2019;48:1083–90. https://doi.org/10.1002/eqe.3165.
[54] Pan C, Jiang J, Zhang R, Xia Y. Closed-form design formulae for seismically isolated structure with a damping enhanced inerter system. Struct Control Health Monit 2021;28:e2840. https://doi.org/10.1002/stc.2840.
[55] Sun H, Zuo L, Wang X, Peng J, Wang W. Exact H-2 optimal solutions to inerter-based isolation systems for building structures. Struct Control Health Monit 2019;26:e2357. https://doi.org/10.1002/stc.2357.
[56] Westermo B, Udwadia F. Periodic response of a sliding oscillator system to harmonic excitation. Earthq Eng Struct Dyn 1983;11:135–46. https://doi.org/10.1002/eqe.4290110111.
[57] Zhao Z, Zhang R, Jiang Y, Pan C. Seismic response mitigation of structures with a friction pendulum inerter system. Eng Struct 2019;193:110–20. https://doi.org/10.1016/j.engstruct.2019.05.024.
[58] De Domenico D, Ricciardi G. Optimal design and seismic performance of tuned mass damper inerter (TMDI) for structures with nonlinear base isolation systems. Earthq Eng Struct Dyn 2018;47:2539–60. https://doi.org/10.1002/eqe.3098.
[59] Zhang RC, Elishakoff I, Shinozuka M. Analysis of nonlinear sliding structures by modified stochastic linearization methods. Nonlinear Dyn 1994;5:299–312. https://doi.org/10.1007/BF00045339.
[60] Tsiavos A, Haladij P, Sextos A, Alexander NA. Analytical investigation of the effect of a deformable sliding layer on the dynamic response of seismically isolated structures. Struct 2020;27:2426–36. https://doi.org/10.1016/j.istruc.2020.08.016.
[61] Hu HS, Nakashima M. Responses of two-degree-of-freedom sliding base systems subjected to harmonic ground motions. J Struct Eng 2017;143. https://doi.org/10.1061/(ASCE)ST.1943-541X.0001653.
[62] Jangid RS. Computational numerical models for seismic response of structures isolated by sliding systems. Struct Control Health Monit 2005;12:117–37. https://doi.org/10.1002/stc.59.
[63] Iura M, Matsui K, Kosaka I. Analytical expressions for 3 different modes in harmonic motion of sliding structures. Earthq Eng Struct Dyn 1992;21:757–69. https://doi.org/10.1002/eqe.4290210902.